Ore Geology Reviews 138 (2021) 104397

Contents lists available at ScienceDirect

Ore Geology Reviews

journal homepage: www.elsevier.com/locate/oregeorev

Igneous genesis of the Bayan Obo REE–Nb–Fe deposit: New petrographical and structural evidence from the H1–H9 cross-section and deep-drilling exploration

Haiyan Tang [a], Yan Liu [b,c,*], Wenlei Song [d,*]

[a] College of Earth Science, Jilin University, Changchun 130061, PR China
[b] Southern Marine Science and Engineering Guangdong Laboratory (Guangzhou), Guangzhou 511458, China
[c] Institute of Geology, Chinese Academy of Geological Sciences, Beijing 100037, PR China
[d] State Key Laboratory of Continental Dynamics, Department of Geology, Northwest University, Xi'an 710069, China

ARTICLE INFO

Keywords:
Petrography
units H1–H9
H8 orebody
Syncline
Igneous genesis
Bayan Obo

ABSTRACT

Rare earth elements (REEs) are a focus of global attention because of their unique properties and high-tech applications. Bayan Obo is the world's largest REE deposit and is hosted in the Paleoproterozoic Bayan Obo Group, Inner Mongolia. The REE resources are concentrated in unit H8, "dolomite marble." However, whether unit H8 has an igneous or sedimentary origin is debated, and relationships among units H1–H9 are unclear, hindering our understanding of the formation of such a giant REE deposit. It was previously assumed that the unit H8 orebody is located in both limbs of the Bayan syncline and unit H9 in the core, which also needs to be confirmed because it is a guide for ore exploration. Field observations and petrographic studies of units H1–H9 were undertaken to re-evaluate the petrology and structure of the Bayan Obo Group. It was found that some units (e.g., H5–H7) are missing from the studied cross-section, with the two sides of unit H9, across the hinge of the so-called syncline, not being directly comparable. Unit H8 displays petrological, mineralogical, and whole-rock REE geochemical characteristics distinct from those of the other units investigated, suggesting they are of different origin. Moreover, deep-drilling exploration indicates major differences between the two limbs of the orebodies in terms of thickness, occurrence, and spatial distribution. The East orebody has a steep dip angle of 70°–80° and continuously extends to depth without reduction of angle, suggesting the syncline is probably nonexistent. These results, combined with the reported intrusion relationship of unit H8 with surrounding rock and *in situ* isotopic studies previously reported, indicate that the orebody is a carbonatitic igneous conduit rather than being of sedimentary origin. SHRIMP U–Pb dating of detrital zircons from the units H2–H9 yielded ages of 2574 ± 25 to 132 ± 2 Ma, overlapping the ages of units H1–H9 and the main REE mineralization periods reported previously. These protracted and complicated ages of the orebody likely represent fluid-aided resetting ages.

1. Introduction

Rare earth elements (REEs) are a focus of global attention because of their importance in low-carbon energy technologies (Chakhmouradian and Wall, 2012; Gunn, 2014; Wall, 2014). Among REE deposits in igneous, metamorphic, and sedimentary (weathering profiles, residual deposits, and placers) host rocks, carbonatite-related light REE (LREE) deposits account for 98% of China's reserves and >33% of global resources (Weng et al., 2015; Xie et al., 2019). China is currently mining three large or giant carbonatite-related REE deposits: the Bayan Obo deposit, the Mianning–Dechang REE belt, and the Weishan deposit (Jia and Liu, 2020). The Bayan Obo deposit, the only giant REE deposit worldwide (Smith et al., 2016) with high-grade reserves of 48 Mt at 6 wt % REE_2O_3 (Drew et al., 1990).

The Bayan Obo deposit is hosted in a sequence of nine Paleo–Mesoproterozoic sedimentary units, H1–H9, of the Bayan Obo Group, with unit H8 hosting most of the REE reserves. It is unresolved whether the H8 orebody is a sedimentary carbonate rock (Meng, 1982; Chao et al., 1992; Yang et al., 2009; Lai et al., 2013) or a carbonatite intrusion (Le Bas et al.,1997; Yang et al., 2003; Xu et al., 2012; Song et al., 2018).

* Corresponding authors at: Southern Marine Science and Engineering Guangdong Laboratory (Guangzhou), Guangzhou 511458, China (Y. Liu). State Key Laboratory of Continental Dynamics, Department of Geology, Northwest University, Xi'an 710069, China (W. Song).
E-mail addresses: ly@cags.ac.cn (Y. Liu), wlsong@nwu.edu.cn (W. Song).

https://doi.org/10.1016/j.oregeorev.2021.104397
Received 18 November 2020; Received in revised form 20 July 2021; Accepted 29 July 2021
Available online 3 August 2021
0169-1368/© 2021 Elsevier B.V. All rights reserved.

Meng (1982) reported the presence of microfossils and several types of laminated sedimentary structures within the H8 orebody, but fossils were not found in later studies (e.g., Fan et al., 2016). Le Bas et al. (1997) suggested that all laminar structures within the orebody were due to tectonic deformation and also found fenite alteration in unit H8, suggesting a igneous carbonatite origin. Recent studies involving *in situ* Sr–Nd–Pb isotopic (Song et al., 2018; Chen et al., 2020), and unconventional Mg (Sun et al., 2012) and B (Kuebler et al., 2020) stable-isotope analyses have favored a carbonatitic origin. Orebody formation has also recently been explained in terms of magmatic processes, including immiscibility and crystallization differentiation (Yang et al., 2019).

The REE mineralization age of the Bayan Obo deposit is debated. Several isotopic systems, including the Sm–Nd, Rb–Sr, U–Th–Pb, Ar–Ar and Re–Os systems, have been applied in whole-rock and mineral orebody dating. Sm–Nd whole-rock and mineral analyses indicate Mesoproterozoic ages, with mineralization occurring mainly at *ca.* 1.3 Ga (Yuan et al., 1992a,b; Cao et al., 1994; Ren et al., 1994; Zhang et al., 2001; Liu et al., 2005). Most Th–Pb rare-earth mineral ages are clustered in the early Paleozoic (0.5–0.4 Ga) (Chao et al., 1991; Wang et al., 1994; Zhang et al., 1994; Zhang et al., 2003; Liu et al., 2004; Hu et al., 2009). Zircons from mineralized dolomite samples have yielded core and rim Th–Pb ages of 1325 ± 60 Ma and 455.6 ± 28.27 Ma, respectively (Campbell et al., 2014). It seems, therefore, that REE mineralization in the Bayan Obo deposit took place over a long time (Song et al., 2018). A recent study by Li et al. (2021) noted that many carbonatite-related REE ore systems have protracted and complicated evolution histories, and the primary REE mineral crystallization age of the Bayan Obo orebody was determined as 1293 ± 48 Ma on the basis of the Sm–Nd geochronometer.

Previous studies have shown that the Bayan Obo deposit occurs in unit H8 dolomite of the Bayan Obo Group in the south limb of the Kuangou anticline, with its morphology and structure being controlled by the Bayan syncline. The core of the Bayan syncline comprises unit H9 black carbonaceous slate, greyish green feldspar slate, and siltstone. A bedded magnetite orebody is hosted in unit H8 dolomite in the south limb of the Bayan syncline (the Dongjielegle iron orebody). The East REE–Fe orebody is in the north limb of the Bayan syncline. It is debated whether the Bayan syncline actually exists (Liu et al., 2006; Zhao, 2014), whether the orebodies in the north and south limbs of the syncline are connected in the core, and whether the ore-forming structure is related to a syncline developed in sedimentary rocks or hydrothermal mineralization. These details have practical significance for exploration, pit design, and scientific study of mineral deposits.

The structure and mineralogy of units H1–H9 and the so-called syncline, as previously reported, lack detailed descriptions, hindering further ore exploration. In recent years, deep-drilling exploration work has been undertaken in the East orebody, which may provide new constraints on the structure and ore resource potential at the Bayan Obo deposit. Therefore, in this study we focused mainly on re-evaluating the petrography, mineralogy, and structure of the orebody in an H1–H9 cross-section investigation and deep-drilling exploration. Together with geochemical analyses and zircon dating, systematic study of the petrography and structure of the ore field should improve understanding of the genesis of this giant REE deposit.

2. Geological setting

The Bayan Obo REE deposit is located in Inner Mongolia, China, and its geology has been detailed described previously (Yang et al., 2009). The deposit is located on the northern margin of the North China Craton, with the basement mainly consists of the Archaean Wutai Group gneisses and migmatites (Chao et al., 1997). The REE-Fe-Nb ores are mainly hosted by the Bayan Obo Group sedimentary rocks, which were considered to be deposited on the continental shelf to the slope of the craton margin. The studied H1–H9 lithological section of the Bayan Obo Group is exposed mainly in the mining area (Zhong et al., 2015; Lai et al., 2016; Liu et al., 2016; Liu et al., 2017; Ren et al., 2019; Fig. 1). Faults in the mining area strike approximately E–W, NNW, NW, NE, and N–S, causing discontinuities in the lithological units (Zhang et al., 2003). The main faults trend near E–W, including the Saiwusu ductile shear zone in the north, the Kuangou Fault, and thrust faults, and a ductile shear zone in the south of the mining area (Zhang et al., 2003; Fig. 1).

As mentioned, the Bayan Obo Group was subdivided into the H1–H9 lithological units in ascending stratigraphic order, with REE mineralization occurring in unit H8 (massive dolomite), which is overlain by unit H9 K-rich slate (Chen et al., 2020). The Bayan Obo deposit comprises three major orebodies, the East, West, and Main orebodies. The Main and East orebodies are related to units H8 and H9 units, and the West orebody is hosted in the H8 unit (Fan et al., 2016; Fig. 2). The H8 dolomite is coarse- to fine-grained (Le Bas et al., 1997; Yang and Le Bas, 2004), with the coarse-grained (>1 mm) parts comprising mainly dolomite and minor rounded, elongate apatite. Most apatite crystals are subprismatic to elongate and oriented to define a lineation due to shearing and deformation (Ren et al., 2019).

Intrusive rocks in the mining area include Mesoproterozoic magmatic carbonatite-related rocks, Precambrian basic-vein rocks, and late Paleozoic intermediate to acidic intrusive rocks exposed over large areas in the south of the mining area (Zhang et al., 2003; Ling et al., 2014). Magmatic carbonatite in the mining area is generally distributed in an E–W direction, extending ~18 km with a width of up to 3–4 km (Fan et al., 2016) (Fig. 1). Intermediate–felsic intrusive rocks in the southeast of the mining area mainly include quartz monzonite, granite, granodiorite, gabbro-diorite, and gabbro. Secondary-ion mass spectrometry zircon U–Pb ages for the granitoids in this area range from 293.8 to 243.2 Ma, indicating formation in a post-collisional environment during the late Permian–Early Triassic (Fan et al., 2009).

3. Sampling and analytical methods

In this study, REE ores in the Bayan Obo H8 orebody were found to occur as massive, banded, and disseminated mineralization. The ore mineral assemblage comprises mainly REE minerals, including monazite and bastnäsite, and gangue minerals such as fluorite, magnetite, barite, and apatite. REE ore is usually banded, and REE minerals occur in fine veins (Fig. 3A, B). In the northeastern part of the main ore, unit H8 intrude unit H9 (Fig. 3C, D), with biotitization and dolomitization near the contact zones. To the north and south of the Bayan Obo deposit, unit H8 also intrudes diorite and granite (Fig. 3E, F). Unit H1 was examined in detail during fieldwork, and samples from units H2–H9 were selected along a cross-section for geochemical and dating analyses (Figs. 4–7). Petrographic, mineralogical, and trace-element studies were undertaken on samples from units H2–H9 to identify their mineral assemblages and for comparison between units to elucidate the detailed geologic and structural characteristics of the ore deposit. Zircons in units H2–H9 were separated for SHRIMP U–Pb dating to further constrain possible hydrothermal activities related to REE mineralization. Analytical methods are described in the Supplementary Material.

4. Results

4.1. Petrographic analyses

Due to extensive alteration, intercalation, and spatial relationships among units H1–H8, with some intruding others, the mineral assemblages are complicated. The results of X-ray powder diffraction (XRD) analysis for samples from units H1–H9 indicate varied mineral compositions (Supplementary Table 1) for units H3–H5 and H7–H9. The results lay a solid foundation for the renaming of units H1–H8.

Mineral compositions were investigated through microscopic examination of samples from units H1–H9 (Figs. 8–10), with some units, particularly H1 and H2 and altered rocks, requiring further study

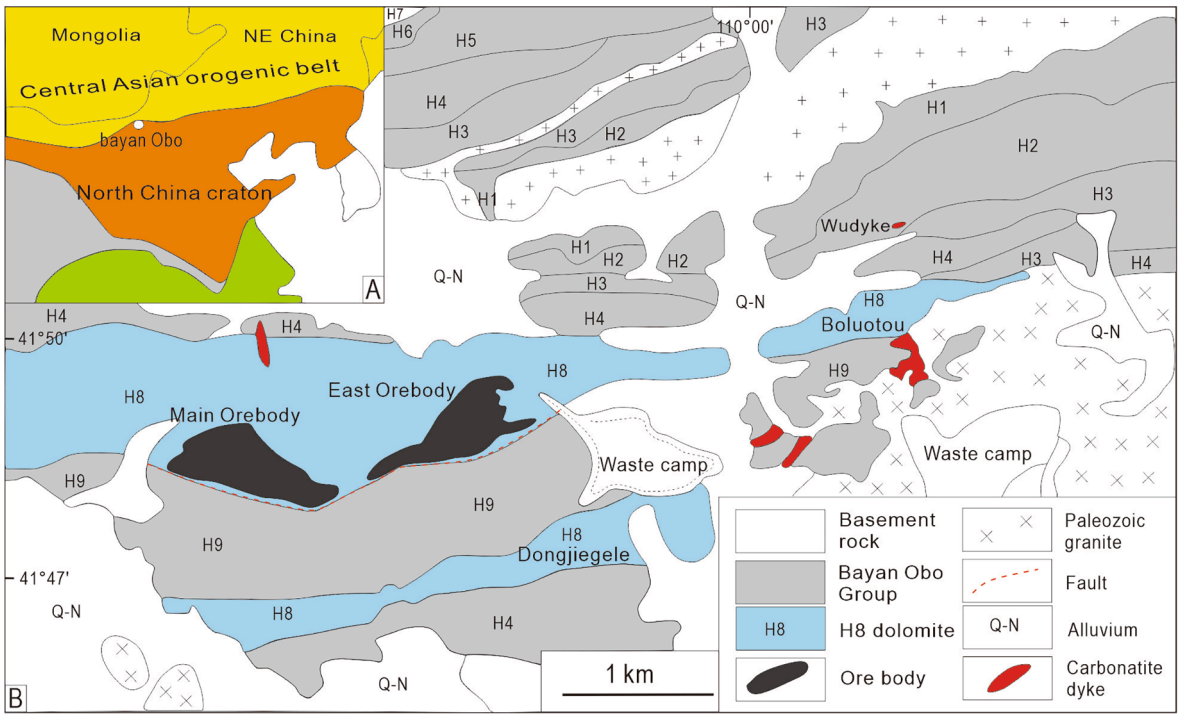


Fig. 1. Simplified geological map showing the major units in the Bayan Obo area (modified from Yang et al., 2011b; Zhang et al., 2017). (A) Location of the Bayan Obo deposit. (B) Intrusive contact between dolomite and calcite carbonatite dykes.

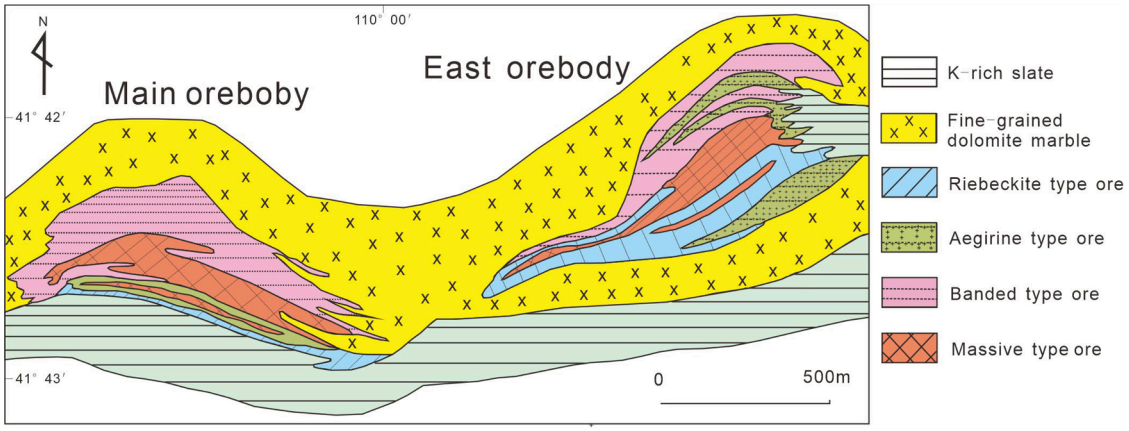


Fig. 2. Geological setting of the Main and East orebodies (modified from Institute of Geochemistry, Chinese Academy of Sciences, 1988).

beyond that reported previously (Li et al., 1996; Zhang et al., 2003; Wang et al., 2019).

Unit H1 comprises quartz sandstone containing >90 vol% quartz with minor feldspar and detritus (Li, 1959; Meng, 1982); it does not occur in the study area (Figs. 4 and 5) but was examined nevertheless. H1 is exposed in the core of the Beikuangou anticline in the Bayan Obo mining area and is a quartzite and quartz sandstone assemblage distal to ore-bearing dolomite (Fig. 1).

The Dulahala Formation in Bayan Obo occurs in the core of the so-called Kuangou anticline in the north of the mining area (Fig. 4). It is distributed in an E–W direction and divided into two sections from top to bottom, with a thickness of >607 m. Its bottom member, chd^{1}, represents unit H1, which is divided into four sub-members based on lithology, with a total thickness of 282 m. Sub-member ch$d^{1\text{-}1}$ is a dark-gray metamorphosed gravel-bearing coarse-grained feldspar–quartz sandstone interbedded with a metamorphosed conglomerate of variable thickness, intercalated with metamorphosed coarse-grained feldspar–quartz sandstone that shows parallel bedding and imbricate structure, 151 m thick. Sub-member ch$d^{1\text{-}2}$ comprises dark-gray metamorphosed medium–coarse-grained feldspar–quartz sandstone and metamorphosed gravel-bearing coarse-grained Na–Fe-diorite–feldspar–quartz sandstone that shows cross-bedding and imbrication. It is in conformable contact with the chd^{1} sub-member, with a thickness of 77 m. Sub-member ch$d^{1\text{-}3}$ comprises dark-gray metamorphosed silty mudstone intercalated with a gray metamorphosed medium–coarse-grained quartz sandstone lens with a structure of interbedding, lenticular and wavy bedding. Sub-member ch$d^{1\text{-}3}$ is in conformable contact with the underlying ch$d^{1\text{-}2}$ sub-member, which has a thickness of 49 m. Sub-member ch$d^{1\text{-}4}$ contains interbedded dark-gray metamorphosed very-coarse-grained feldspar–quartz sandstone and metamorphosed coarse-grained feldspar–quartz sandstone that shows parallel bedding and erosion structures. It is in conformable contact with the underlying ch$d^{1\text{-}3}$ sub-member, which has a thickness of >5 m (Fig. 6).

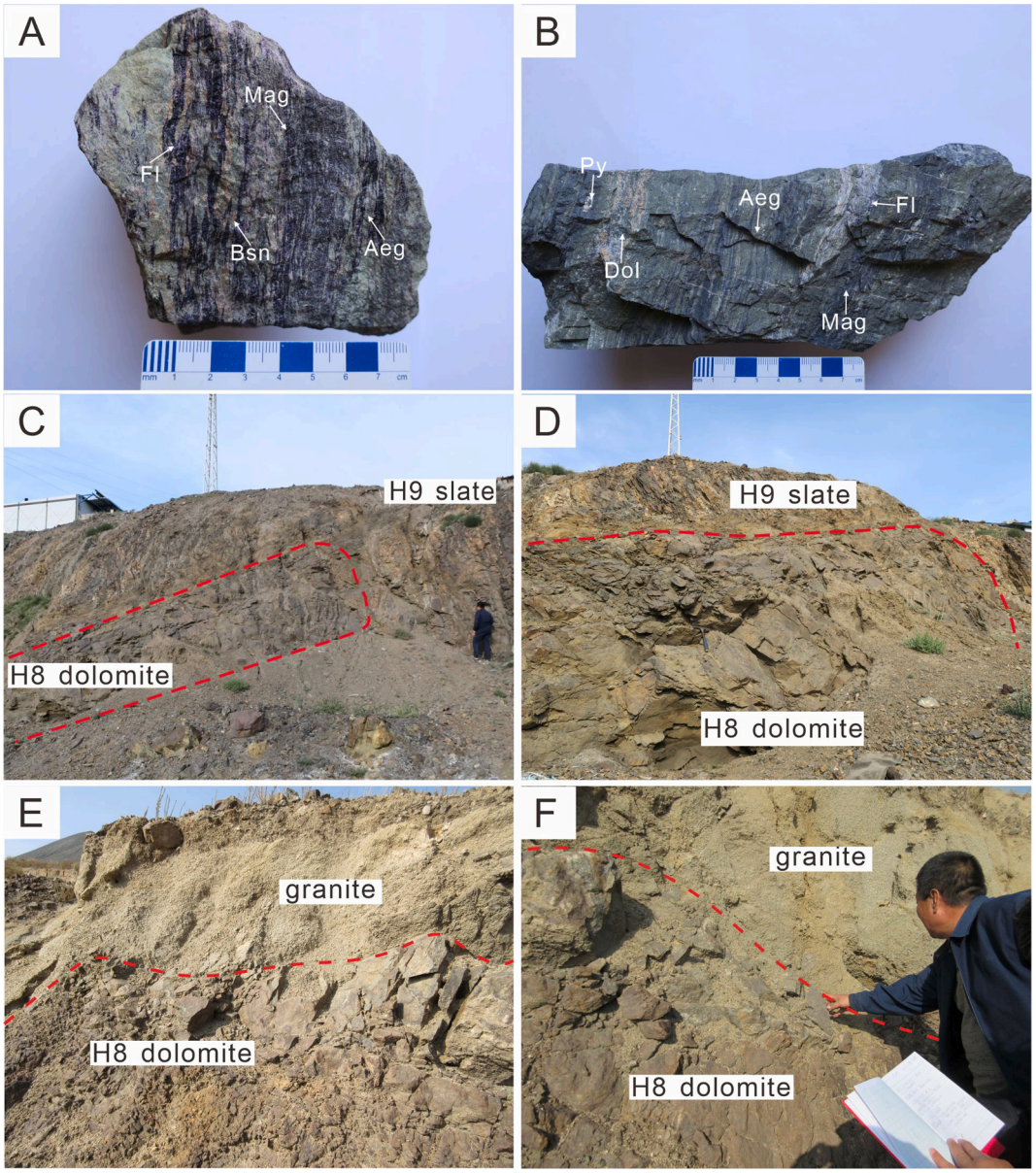


Fig. 3. Banded REE ores from unit H8 and the relationship between units H8 and H9 (with H8 intruding H9). (A, B) Banded REE ores in unit H8; (C, D) dolomite in unit H8 intruding unit H9; (E, F) unit H8 intruding diorite and granite in the north and south of the Bayan Obo deposit. Abbreviations: Dol, dolomite; Fl, fluorite; Mag, magnetite; Aeg, aegirine; Py, pyrite; Hem, hematite.

The upper member of the Dulahala Formation, chd^{2}, formerly classified as unit H2, is divided into three sub-members with a total thickness of 325 m. Sub-member ch$d^{2\text{-}1}$ comprises dark-gray metamorphosed fine-grained feldspar–quartz sandstone with low-angle bedding, in conformable contact with the ch$d^{1\text{-}4}$ sub-member, with a thickness of 45 m. Sub member ch$d^{2\text{-}2}$ comprises grayish-white metamorphosed fine-grained quartz sandstone that shows aeolian cross-bedding, in conformable contact with the ch$d^{2\text{-}1}$ sub-member, with a thickness of 156 m. Sub member ch$d^{2\text{-}3}$ comprises grayish-white metamorphosed quartz sandstone with bidirectional cross-bedding in conformable contact with the underlying ch$d^{2\text{-}2}$ sub-member, with a thickness of 124 m (Fig. 6). Thus, H1 is mainly composed of quartz sandstone.

Microscope observation revealed that minerals in units H2–H9 are fine-grained and cannot be clearly recognized (Fig. 8). These samples were therefore examined by BSE imaging (Fig. 9).

Sample BY94-15 in H2 unit has a granular crystalloblastic structure, partial residual sandy texture with massive structure. It comprises mainly quartz with minor zircon and opaque dark minerals, with the latter distributed in gaps in the former. The protolith is mainly quartz sandstone with a special structure possibly formed during regional metamorphism (Fig. 8A). Quartz has an irregular granular form, with grain sizes of 0.02–0.95 mm and amount of about 95 vol%. Small amounts of fine-grained magnetite, K-feldspar, and plagioclase also occur (Fig. 9A). Ellipsoidal zircon grains are occasionally observed, with a grain size of ~0.10 mm. Together with field observation, H2 unit is mainly composed of quartz sandstone and quartzite.

Sample BY94-14 in H3 unit is a slate derived from argillaceous rocks with residual metamorphic platy texture, comprising mainly clay minerals (80 vol%), quartz (5 vol%, including some veinlets), sericite (5 vol %), and minor opaque minerals (<5 vol%). The quartz is allomorphic granular and silt-sized; sericite appears as small scales; clay minerals have an aphanitic texture, and some opaque minerals appear as dots or clumps (Fig. 9B).

Sample BY94-19 in H3 unit has residual metamorphic argillaceous structures and platy textures and comprise mainly quartz (≤7 vol%), sericite (≤13 vol%), clay minerals (56 vol%), and opaque minerals (≤24

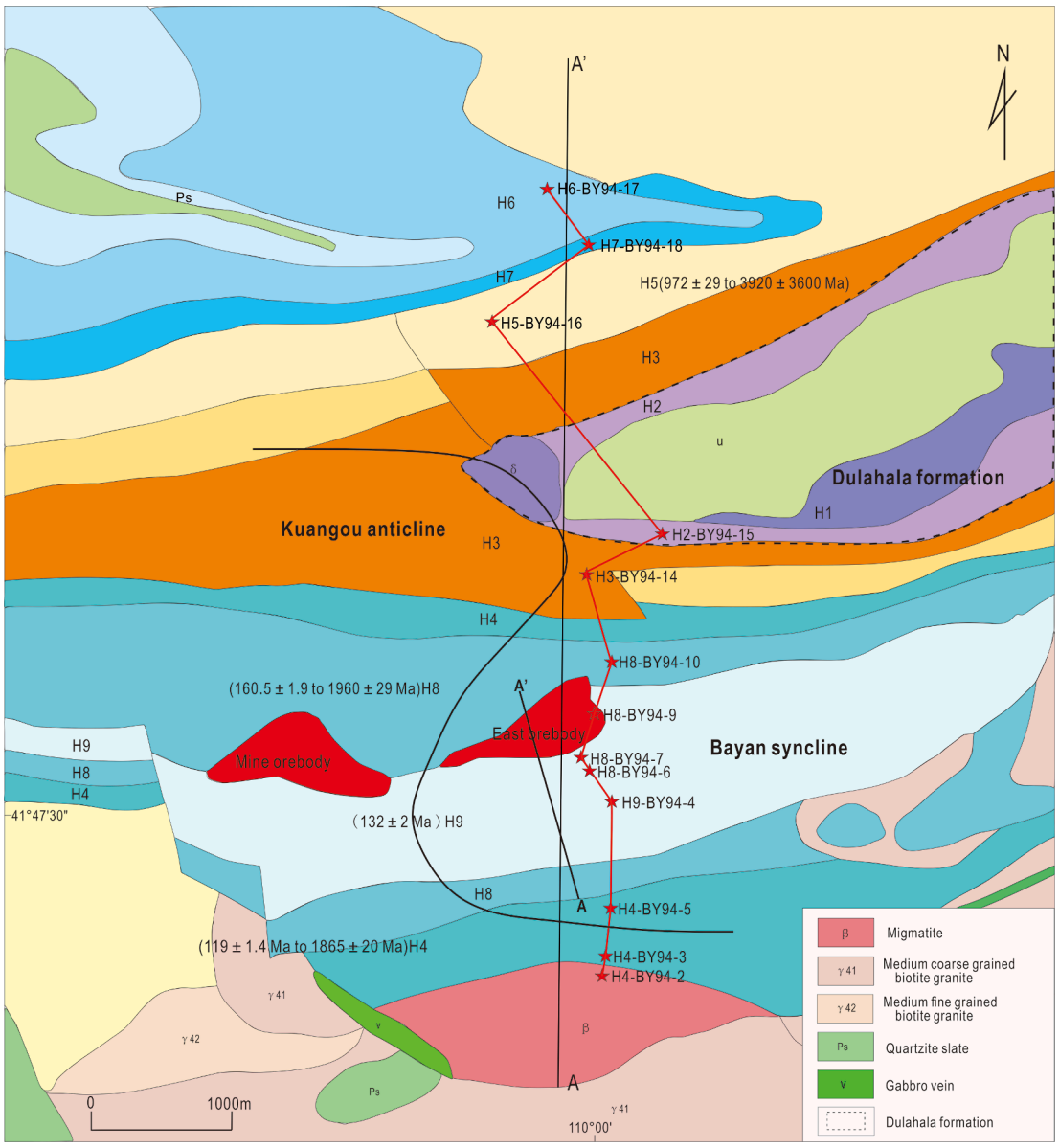


Fig. 4. Cross-section of the eastern part of the East and Main orebodies, showing sample locations and units.

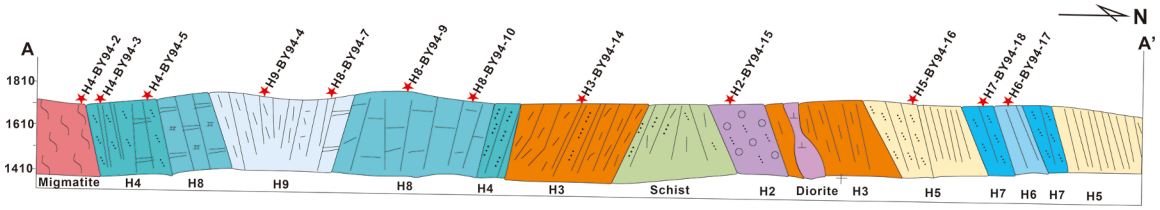


Fig. 5. Cross-section A–A' of the eastern part of the East and Main orebodies in Fig. 4, showing sample locations and units.

vol%). The minerals are very fine-grained, with low degrees of recrystallization (Fig. 8B). Quartz is allomorphic granular and silt-sized; sericite, phlogopite, and albite have a similar grain size and occur as small scales. Clay minerals are cryptocrystalline. Opaque minerals such as ilmenite are distributed as star-shaped dots and clumps (Fig. 9B). Then, H3 unit is mainly composed of argillaceous slate.

Sample BY94-2 in H4 unit is siliceous slate with a granular crystalloblastic and massive structure. It comprises mainly quartz (68 vol%) with a grain size of 0.03–0.82 mm, K-feldspar (23 vol%; 0.06–1.31 mm), and aegirine (6 vol%; 0.04–0.32 mm), followed by epidote, apatite, and opaque metal minerals (Fig. 8C). Some albite and glaucophane also occur with irregular shape in sample BY 94-3 of unit H4 (Fig. 9C). Together with other samples in H4, H4 unit is mainly composed of siliceous slate.

Sample BY94-16 in H5 unit is slate derived from argillaceous rocks with residual platy metamorphic mineral textures, comprising mainly clay (55 vol%) and carbonate (10 vol%, including some veinlets) minerals, biotite (10 vol%), and minor opaque minerals (<5 vol%) (Fig. 8D).

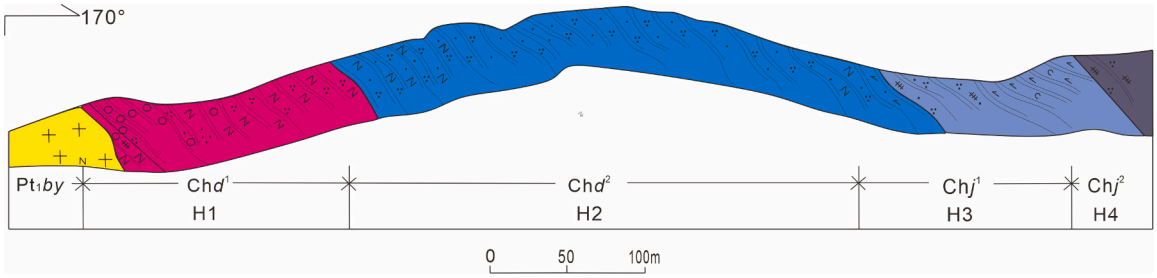


Fig. 6. Cross-section of units H1–H4.

The quartz is allomorphic granular and silt-sized; biotite and some albite occur as small scales (Fig. 9E); clay minerals have an aphanitic texture, and some opaque minerals appear as dots or clumps. Such samples in H5 unit could be classified as carbonatized argillaceous slate.

Sample BY94-17 in H6 unit is metamorphosed quartz sandstone affected by carbonatization. It has a blastopsammitic texture and comprises mainly quartz (80 vol%) and carbonate (10 vol%) minerals, sericite (5 vol%), and minor opaque minerals (<5 vol%). Quartz grains are irregular in shape with diameters of 0.02–0.82 mm; carbonate minerals are irregular in shape and occur between detrital quartz grains; sericite appears as small scales (Fig. 8E). Such samples are classified as carbonatized and metamorphosed fine-grained quartz sandstone or metamorphosed medium–fine-grained quartz sandstone. Smithsonite occurs occasionally in such samples (Fig. 9F). H6 unit is mainly composed of metamorphic medium-fine grained quartz sandstone.

Sample BY94-18 in H7 unit has a microcrystalline texture and blocky structure, and comprises mainly calcite minerals (85–90 vol%) and quartz (10–15 vol%), with minor opaque minerals (<2 vol%). It is characterized by high contents of fine calcite minerals and hydrothermal calcite veins. Microcrystalline calcite minerals have grain sizes of <0.05 mm and are irregular in shape. Opaque minerals are distributed as star dots and clumps (Fig. 8F). Such samples are regarded as microcrystalline limestone.

Samples BY94-7 and BY94-10 in H8 unit have granular crystalloid textures and massive structure and are typical REE ores comprising mainly calcite (93 vol%) as veins and matrix grains (0.01–0.23 mm), with minor opaque minerals (up to 7 vol%) (Fig. 8G). H8 samples comprise mainly coarse-grained carbonatite, altered fine-grained carbonatite, and quartzite altered by fragmentation–-fluorization–epidotization and overlapped by REE mineralization.

Sample BY94-5 in H9 unit has cryptocrystalline texture and massive structure. It comprises mainly quartz (92 vol%) with irregular granular shapes of grain size < 0.24 mm, followed by ribbon-like opaque dark minerals (8 vol%). Most minerals are cryptocrystalline (Fig. 8H). Opaque dark minerals are occasionally observed, distributed in the form of a star or ribbon, with organic-matter contents of ~8 vol%.

Sample BY94-4 in H9 unit has a variegated silty texture and slaty structure, and comprises mainly quartz (89 vol%), chloritoid (6 vol%), and glaucophane (4 vol%), with minor opaque metallic minerals. Such samples are classified as silty slate or chloritoid silty slate (Fig. 9G–H). Quartz grains have irregular shapes with grain sizes of 0.02–0.38 mm; chloritoid is euhedral to subhedral and columnar, with grain sizes of 0.06–0.55 mm; glaucophane has an irregular shape with grain sizes of 0.07–0.13 mm. Albite and magnetite with irregular shape are occasionally observed (Fig. 9G). In some sample domains, euhedral or subhedral chloritoid occurs together with aggregates of radial or fascicular chloritoid crystals (~16 vol%). Fine-grained zircons also occur in these samples (Fig. 9H). Mineral assemblages and texture in H9 unit is very complicated (Yuan et al., 1995) and could be classified as a type of slate.

4.2. Petrographic studies of unit H8 and geochemistry of units H2–H9

Overlying the lower sequence of units H1–H7 units is the dominant ore-bearing unit H8, occurring mainly in the footwall of orebodies (Figs. 4–6). The results of XRD analyses of typical Bayan Obo ores indicate that these samples have similar gangue and REE mineral assemblages. Primary REE minerals in the deposit are bastnäsite and monazite. Most REE minerals are fine-grained (<2 mm), occasionally with coarse-grained (<10 mm) fluorite. Gangue minerals include mainly fluorite, quartz, calcite, and barite, with similar mineral compositions across samples. XRD, microscopic, and SEM–BSE observations (Supplementary Table 1; Figs. 8–10) also indicate that unit H8 comprises dolomite, calcite, fluorite, barite, and bastnäsite, and other alteration minerals such as proxygene and amphibole, which are rare in the other units. This distinction between H8 and the other units is consistent with its being the main REE mineralization unit. The other units contain large amounts of plagioclase, amphibole, dolomite, K-feldspar, quartz, pyroxene, chlorite, illite, and pyrite; these minerals are scarce in unit H8.

The alteration, hydrothermal gangue minerals, and REE mineralization generally occur in dolomite in the Bayan Obo deposit, with large amounts of fluorite overprinting dolomite as veinlets with widths of <100 μm, or occurring as scattered massive fluorite (Fig. 10A). Barite overprints fluorite and dolomite, and therefore crystallized later (Fig. 10B). The REE mineralization is closely associated with fluorite, barite, and dolomite, with these and other hydrothermal minerals overlapped by REE mineralization (Fig. 10C, D). Fluorite is a primary gangue mineral associated with REE mineralization in the Bayan Obo deposit and occurs in colorless, green, and purple varieties. It is typically oval, up to ~2 cm in diameter, and occurs with other coarse-grained minerals of 2–5 cm diameter in fluorite veinlets. Bastnäsite, the most important REE minerals in the Bayan Obo deposit, occurs in a wide variety of assemblages, primarily due to multiple generations of formation (Fig. 10B–E). Monazite occurs as aggregations or single columnar crystals in fissures among apatite, britholite, and calcite (Fig. 10F).

Unlike most carbonatite-related REE deposits worldwide (Broom-Fendley et al., 2016; Liu et al., 2019a,b; Liu and Hou, 2017; Xu et al., 2015), the Bayan Obo deposit includes both Fe and REE mineralization, but the relationship between the two is unclear. Bulk massive magnetite is usually distributed in dolomite, with no apparent connection with fluorite, barite, or other hydrothermal gangue minerals (Fig. 10). Some REE minerals overprint magnetite, suggesting that REE mineralization occurred continuously over a relatively long period.

Based on rock types and their REE contents (Table 1), samples were divided into two subgroups: unit H8 (samples BY94-7, BY94-9, and BY94-10) with very high ΣREE contents of 19,327–30,093 ppm; and the remaining samples of units H3–H5, H7, and H9 with relatively low ΣREE contents of 23–1349 ppm. Unit H8 samples are enriched in P, consistent with the high apatite abundance of dolomite rock, while other samples are depleted in P. Unit H8 samples are also enriched in Ba, Th, and light REEs (LREEs) but depleted in Nd (Fig. 11). All samples in these units have high $(La/Yb)_N$ ratios with obvious LREE/heavy REE (HREE) fractionation and no apparent Eu anomalies, suggesting REE mineralization occurred mainly in unit H8.

Based on this and previous studies (e.g., Li et al., 1996; Zhang et al., 2003; Wang et al., 2019), the lithology of units H1–H9 may be

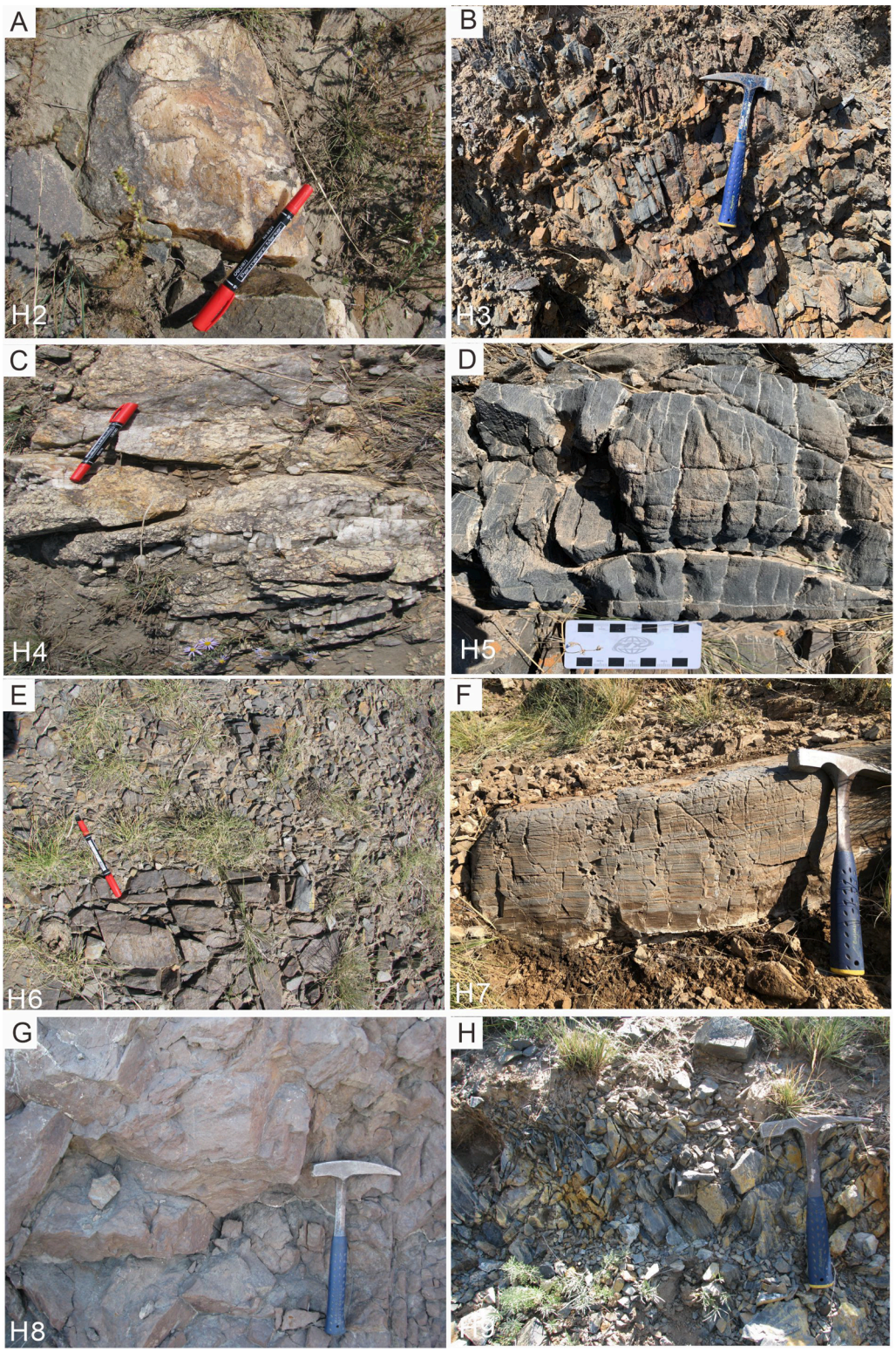


Fig. 7. Occurrence and field observations of units H2–H9 (A–H, respectively).

summarized as follows. Unit H8 samples are enriched in La, Ce, Sm, and P, with high Sr and Ba contents, distinguishing them from samples from other units. They have high ΣREE contents, HREE contents of 189–221 ppm, and LREE/HREE ratios of 101–135. LREE/HREE fractionation is indicated by their $(La/Yb)_N$ ratios of 1212–2254. In most carbonatite-related REE deposits or fertile carbonatites, carbonatite is enriched in Sr, Ba, and REE, as in the Mianning–Dechang (Hou and Cook, 2009), Weishan (Jia and Liu, 2019), Qieganbulake (Ye et al., 2013), and Mountain Pass (Castor, 2008) deposits. In the remaining units, ΣREE contents are in the range of 23.8–1349 ppm, with LREE contents of 21.4–1333 ppm, HREE contents of 1.4–221 ppm, LREE/HREE ratios of 15.3–90.2, and $(La/Yb)_N$ ratios of 14.0–253; with little LREE/HREE fractionation. These results indicate that unit H8 has petrological, mineralogical, and whole-rock geochemical characteristics distinct from

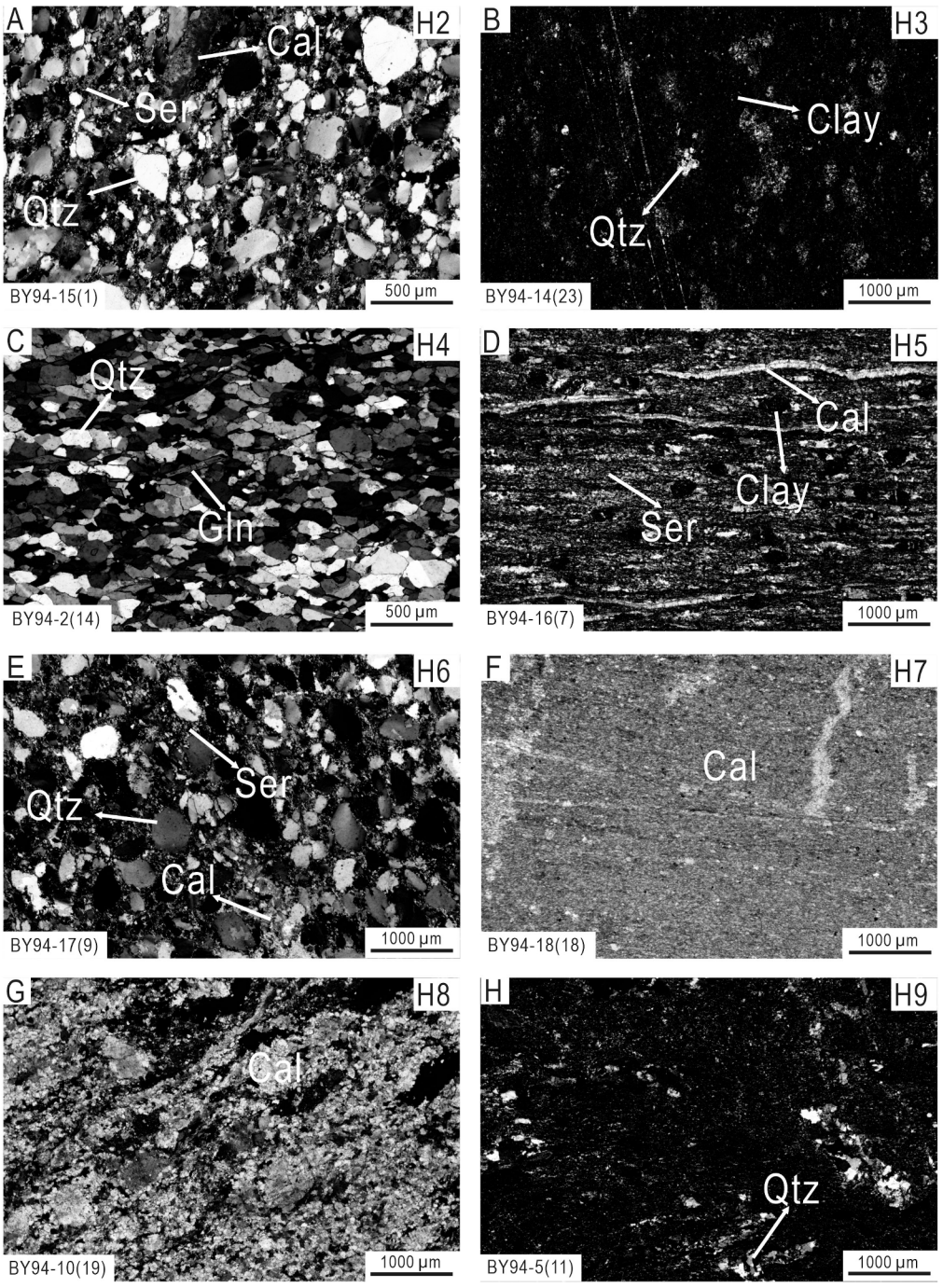


Fig. 8. Photomicrographs of samples from units H2–H9 and their lithology. (A) Quartz sandstone in H2 unit is predominate of quartz with irregular granular form, grain size of 0.02–0.95 mm and amount of about 95 vol. %; (B) A argillaceous slate in H3 unit has residual metamorphic argillaceous structures and platy textures and comprises mainly quartz (≤7 vol.%), sericite (≤13 vol.%), clay minerals (56 vol.%), and opaque minerals (≤24 vol.%); (C) Siliceous slate in H4 unit has a granular crystalloblastic and massive structure. It comprises mainly quartz (68 vol.%) with a grain size of 0.03–0.82 mm, K-feldspar (23 vol.%; 0.06–1.31 mm), aegirine (6 vol. %; 0.04–0.32 mm) and minor epidote, apatite, and opaque metal minerals; (D) Carbonatized argillaceous slate in H5 unit has residual platy metamorphic mineral textures and comprise mainly clay (55 vol.%), carbonate (10 vol.%, including some veinlets) minerals, biotite (10 vol.%), and minor opaque minerals (<5 vol.%); (E) Metamorphic medium-fine grained quartz sandstone in H6 unit has a blastopsammitic texture and comprises mainly quartz (80 vol.%), carbonate minerals(10 vol.%), sericite (5 vol.%), and minor opaque minerals (<5 vol.%); (F) Microcrystalline limestone in H7 unit has a microcrystalline texture and blocky structure, and comprises mainly calcite minerals (85–90 vol.%) and quartz (10–15 vol.%), with minor opaque minerals (<2 vol.%). Microcrystalline calcite minerals have grain sizes of <0.05 mm and are irregular in shape; (G) REE ore in H8 unit have granular crystalloid textures and massive structure and comprise mainly calcite (93 vol.%) as veins and matrix grains (0.01–0.23 mm), with minor opaque minerals (up to 7 vol.%). Such ore samples comprise mainly coarse-grained carbonatite, altered fine-grained carbonatite, and quartzite altered by fragmentation–fluorization–epidotization and overlapped by REE mineralization; (H) Slate in H9 unit has crypto-crystalline texture and massive structure. It comprises mainly quartz (92 vol.%) with irregular granular shapes of grain size <0.24 mm, followed by ribbon-like opaque dark minerals (8 vol.%). Most minerals are cryptocrystalline. Alb, albite; Ap, apatite; Bt, Biotite; Cal, calcite; Gl, glaucophane; Kfs, K-feldspar; Mag, magnetite; Phl, phlogopite; Pl, plagioclase; Qtz, quartz.

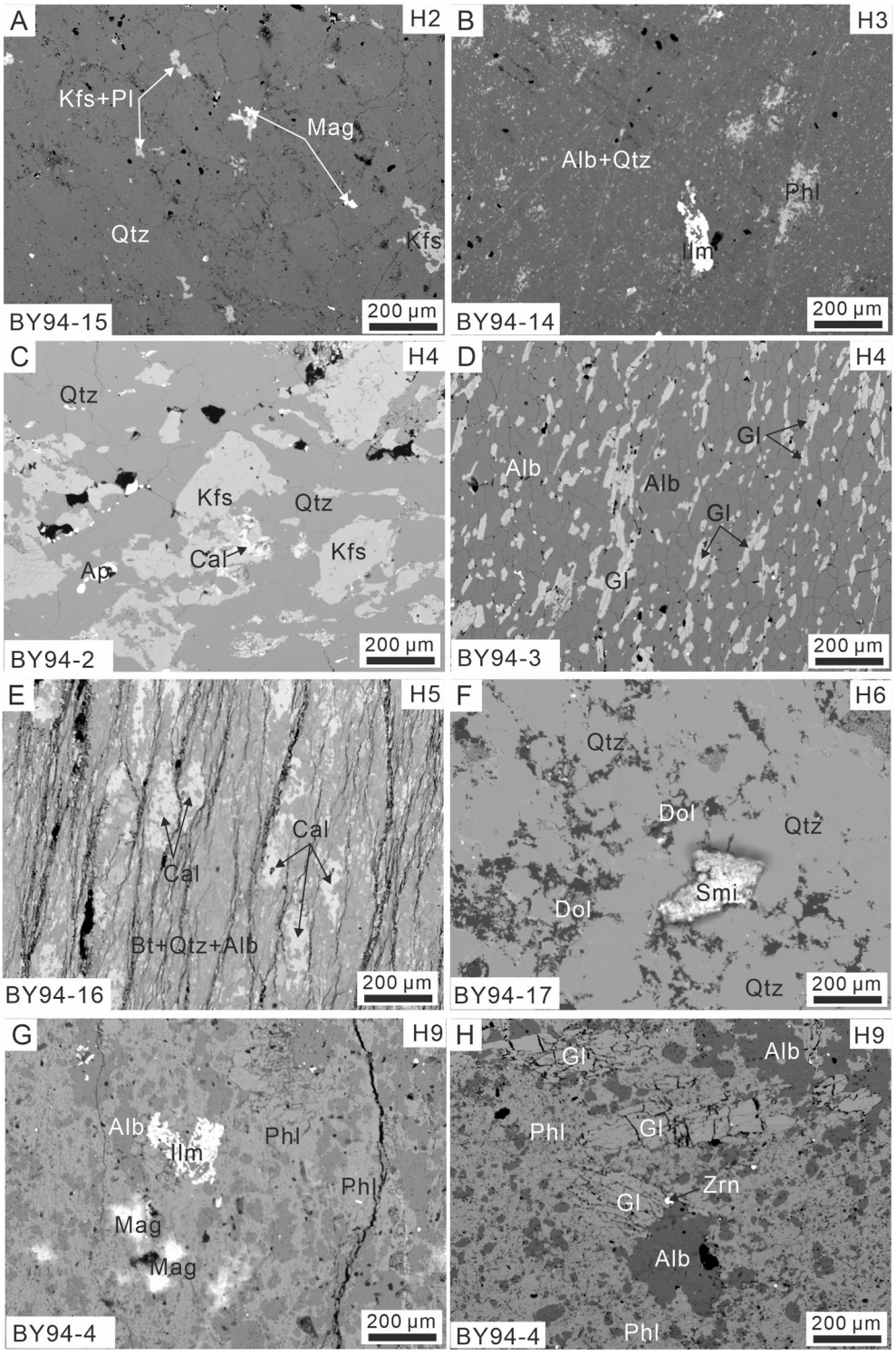


Fig. 9. Backscattered-electron images of samples from units H2–H9. (A) Quartzite overprinted by magnetite, K-feldspar, and plagioclase; (B) phlogopite and ilmenite in argillite; (C) quartz sandstone comprising mainly quartz with some massive K-feldspar overprinted by apatite and calcite; (D) quartz sandstone comprising mainly quartz with albite and glaucophane, suggesting hydrothermal activity; (E) massive calcite overprinting dark slate, with biotite and albite occurring in fissures in dark slate; (F) massive or irregular dolomite, smithsonite, and albite in quartz sandstone; (G) massive phlogopite, ilmenite, and albite overprinting chlorite slate; (H) glaucophane, albite, and phlogopite overprinting chlorite slate. Alb, albite; Ap, apatite; Bt, Biotite; Cal, calcite; Dol, dolomite; Gl, glaucophane; llm, ilmenite; Kfs, K-feldspar; Mag, magnetite; Phl, phlogopite; Pl, plagioclase; Qtz, quartz; Smi, smithsonite; Zrn, zircon.

those of other units investigated. The mineralogy and geochemistry of the orebody are similar to those of typical REE mineralization carbonatites, suggesting that unit H8 is likely of carbonatitic origin.

4.3. SHRIMP U–Pb dating

Most zircons from unit H1–H9 samples are euhedral, 10 × 20 μm to 50 × 100 μm in size, and exhibit oscillatory CL zoning. Some zircons display a bright domain, possibly due to fluid alteration. Neither fluid nor mineral inclusions were visible in CL images (Fig. 12). SHRIMP U–Pb dating was undertaken for zircon grain samples from units H2–H9. It has been reported that zircons with U contents of >2500 ppm often display progressive increases in radiogenic $^{206}Pb/^{238}U$ ratios and apparent ages, with increasing U content due to U-dependent changes in sputtering and secondary-ionization efficiency during SHRIMP U–Pb analysis (White and Ireland, 2012). Such samples were excluded from age calculations.

Zircon dating results for rock samples from units H3, H4, H8, and H9 are summarized in Supplementary Table 2. Twelve analyses of H3 samples yielded ages of 2574 ± 25 to 972 ± 29 Ma. Most H4 zircons

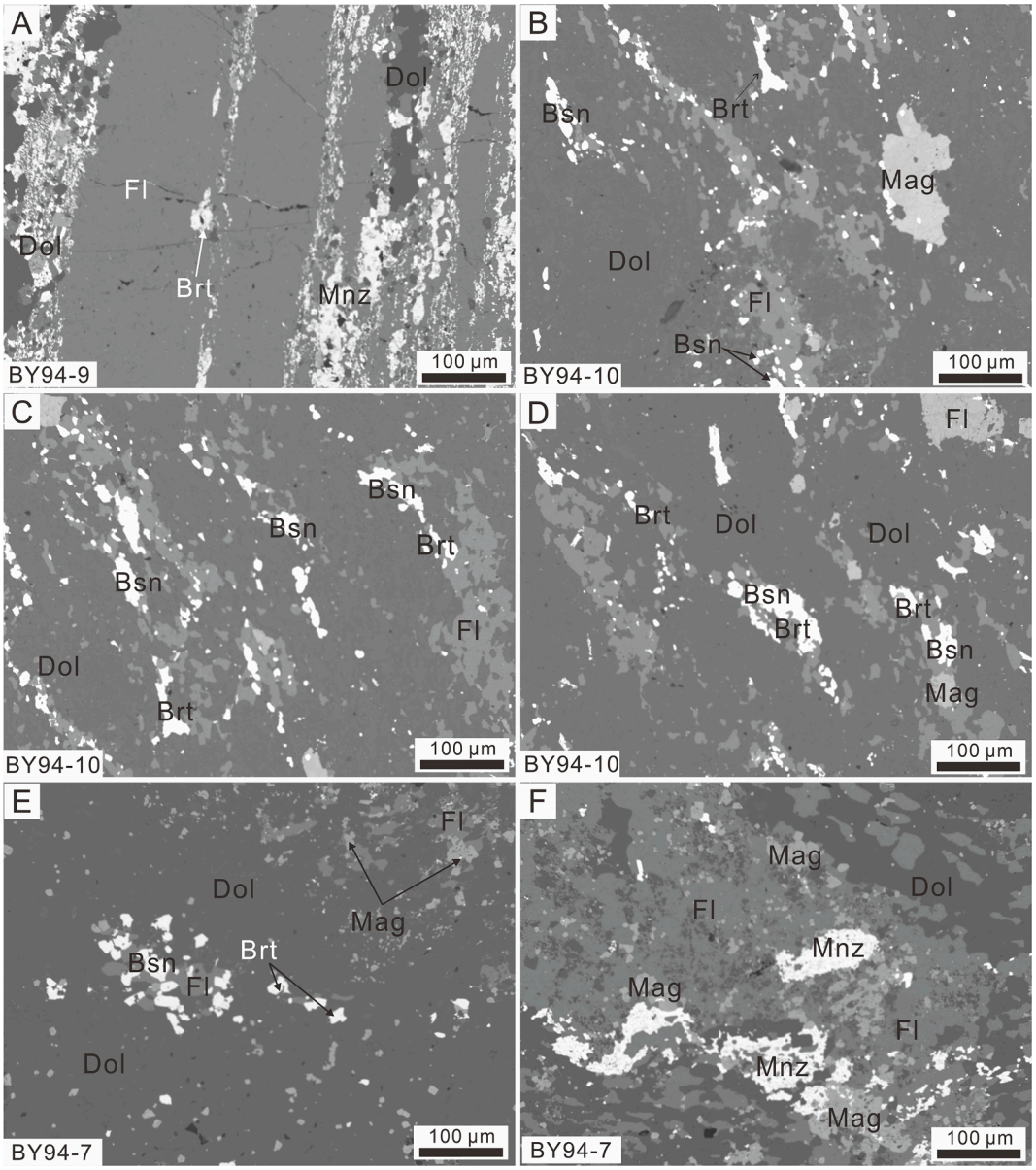


Fig. 10. Backscattered-electron images of samples from unit H8. (A) Fluorite overprinting dolomite overprinted by barite, with monazite overprinting both; (B) barite, magnetite, fluorite, and bastnäsite overprinting dolomite and magnetite, with fluorite overprinted by bastnäsite; (C) fluorite overprinting dolomite overprinted by barite, with both overprinted by bastnäsite; (D) barite, magnetite, fluorite, and bastnäsite overprinting dolomite and magnetite, with fluorite overprinted by bastnäsite; (E) barite, magnetite, fluorite, and bastnäsite overprinting dolomite and magnetite, with fluorite overprinted by bastnäsite; (F) fluorite overprinting dolomite overprinted by barite, with both overprinted by monazite. Brt, barite; Bsn, bastnäsite; Dol, dolomite; Fl, fluorite; Mnz, monazite; Mag, magnetite.

have ages of 1865 ± 20 to 240.2 ± 2.8 Ma. H8 zircons yielded ages of 2523 ± 28 to 157.2 ± 1.9 Ma. Eleven H9 analyses yielded a concordant age of 132 ± 2 Ma (mean-squared weighted deviation [MSWD] = 2.7; Fig. 13). SHRIMP U–Pb dating of detrital zircons from the units H2–H9 thus yielded an extensive range of ages, from 2574 ± 25 to 132 ± 2 Ma (Fig. 14).

4.4. Borehole description

Borehole WK22-02 is in the core area of the Bayan syncline (Fig. 15) in the East orebody, with an opening angle of 89° and direction 342°, and a depth of 1506 m. Borehole samples indicate that the upper 807 m is slate (H9), comprising mainly siliceous (K-rich) and carbonaceous slate that is free of Fe and REE mineralization. The borehole penetrates dolomite below 807 m and extends to 1506 m depth. The whole dolomite section contains REE mineralization, with an average content of 4.63%. The magnetite orebody also occurs in this section at 1140–1222 m depth, with a grade of up to 50%.

Borehole WK22-60 is in the core of the Bayan syncline (Fig. 15), with an opening angle of 89° and direction of 162.5°, and there are plans to drill into the Dongjiegele orebody to a depth of 862 m. Core samples indicate that the slate section (unit H9) extends from the surface to a depth of 107 m, and comprises mainly siliceous and carbonaceous slate, free of Fe and REEs. The borehole penetrates dolomite between 107 m and 856 m. The dolomite section contains REE resources with an average content of 3.56%, with no obvious magnetite enrichment.

The orebody exploration profile on line 22 and a comparison of data from the WK22-02 and WK22-60 boreholes indicated that it was difficult to correlate the orebodies owing to the subsurface structural constraints of the syncline. The Dongjielegle Fe orebody extends to the south in the inferred core area and a major syngenetic fault is present in the upper Fe orebody, which extends downward almost vertically with a tendency to

Table 1
REE and trace element compositions of H3-H9 units in the Bayan Obo deposit.

Sample No.	BY 94-3	BY 94-4	BY 94-5	BY 94-7	BY 94-10	BY 94-14	BY 94-16	BY 94-18	BY 94-19
Unit	H4	H9	H4	H8	H8	H3	H5	H7	H3
Rb	2.50	74.7	182	0.40	1.30	225	51.5	7.90	286
P	131	171	218	2575	1833	43.7	175	131	349
Sr	152	41.9	154	3150	1770	201	304	139	133
Ba	2415	679	1665	4140	9100	3970	166	399	2030
Th	2.32	2.58	9.12	137	125	1.76	6.96	5.30	25.0
U	3.66	0.58	0.58	0.40	0.50	0.64	0.61	4.57	3.07
Nb	68.6	187	141	403	377	35.0	8.10	15.1	25.4
Zr	148	199	220	5.50	5.50	26.0	24.0	22.0	229
Hf	3.40	5.50	5.30	0.50	0.20	0.90	0.70	0.50	6.60
Ti	0.17	0.14	0.29	0.10	0.07	0.35	0.08	0.02	0.43
La	63.8	12.3	120	4730	9740	4.70	55.7	364	144
Ce	165	26.9	275	12,700	17,950	9.20	119	682	303
Pr	17.4	2.89	28.0	1300	1655	0.99	12.1	64.4	29.8
Nd	47.6	9.10	82.9	<1.00	2.00	5.10	38.9	202	88.3
Sm	4.73	1.19	9.63	347	448	1.02	3.91	17.2	12.4
Eu	0.85	0.21	1.84	60.8	77.4	0.35	0.92	3.5	2.62
Gd	1.63	0.52	3.34	116	140	0.5	2.54	7.34	8.30
Tb	0.17	0.05	0.32	12.6	15.1	0.06	0.34	0.84	1.24
Dy	0.72	0.19	1.45	42.5	46.5	0.31	2.04	4.24	7.06
Ho	0.11	0.04	0.21	5.34	5.72	0.06	0.37	0.66	1.45
Er	0.25	0.14	0.48	8.80	9.30	0.18	1.02	1.75	4.03
Tm	0.04	0.03	0.06	0.75	0.75	0.03	0.14	0.22	0.60
Yb	0.35	0.27	0.34	2.80	3.10	0.24	0.95	1.20	3.72
Lu	0.09	0.06	0.05	0.28	0.33	0.05	0.12	0.18	0.58
Y	2.60	1.10	4.5	120	132	1.60	10.3	20.3	39.8
$(La/Yb)_N$	130	32.9	253	1212	2254	14.0	42.1	217	27.8
$(La/Sm)_N$	8.44	6.47	7.79	8.53	13.6	2.88	8.91	13.2	7.26
δEu	0.94	0.82	0.99	0.93	0.94	1.50	0.89	0.95	0.79
δCe	1.21	1.11	1.16	1.26	1.1	1.05	1.12	1.09	1.13
ΣREE	303	53.9	523	19,327	30,093	22.8	237	1349	607
LREE	299	52.6	517	19,138	29,872	21.4	230	1333	580
HREE	3.32	1.27	6.19	189	221	1.40	7.38	16.2	26.4

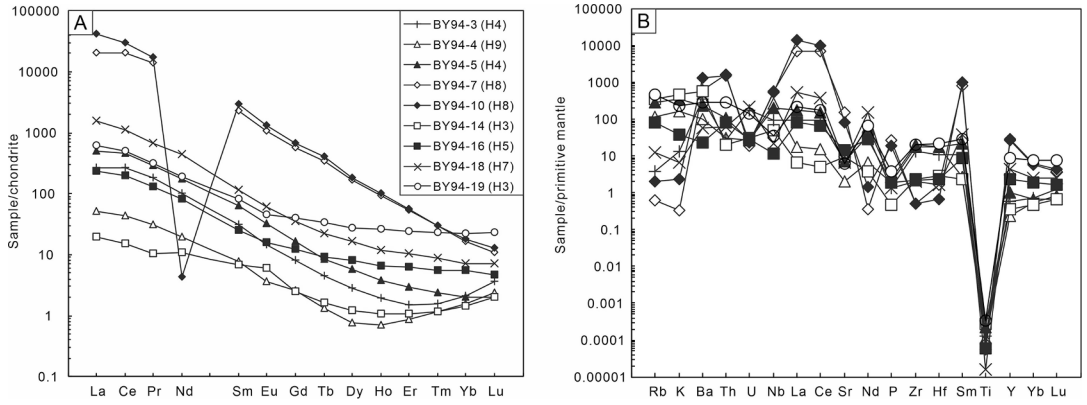


Fig. 11. (A) Primitive-mantle-normalized trace-element and (B) chondrite-normalized REE variation diagrams for samples from units H2–H9.

dip to the south at depth. In terms of shape and appearance, the Dongjielegle orebody is narrow and disseminated compared with the East orebody, which has a more complete structure. The two orebodies are very different in terms of scale, occurrence, and spatial form, so it is difficult to correlate them at depth.

In the WK22-02 borehole in the East Bayan orebody, the orebodies occur at depths of 1140–1222 m, different to the orebody distribution elsewhere in the syncline (orebodies are found at ~800 m in the syncline core). The dip of the strata does not change substantially throughout the borehole (it is consistently inclined southward), and the syncline structural style is inconsistent with the structural characteristics of the syncline. After the drilling, the strike of the ore body provides a clear direction for future deep prospecting, and differs from previous understanding. From the cross-section of the East and Dongjiegele orebodies, the deep occurrence of dolomite revealed by borehole WK22-02 is inconsistent with that revealed at the surface of borehole ZK22-60. The dolomite at the surface inclines to the north, whereas that which occurs in the in deep strata inclines to the south. This cannot be explained by current stratigraphic and structural syncline models, with there being little evidence of a syncline.

5. Discussion

5.1. Evidence for the absence of Bayan syncline

The deposit, hosted by the Bayan Obo Group, is thought to include units H1–H9, from bottom to top. However, the distribution of these units is irregular and complicated, with intrusions occurring between them (Li et al., 1996; Zhang et al., 2003; Fan et al., 2016; Wang et al., 2019).

Based on this and previous studies (Li et al., 1996; Zhang et al., 2003; Fan et al., 2016; Wang et al., 2019), the Bayan Obo Group can be

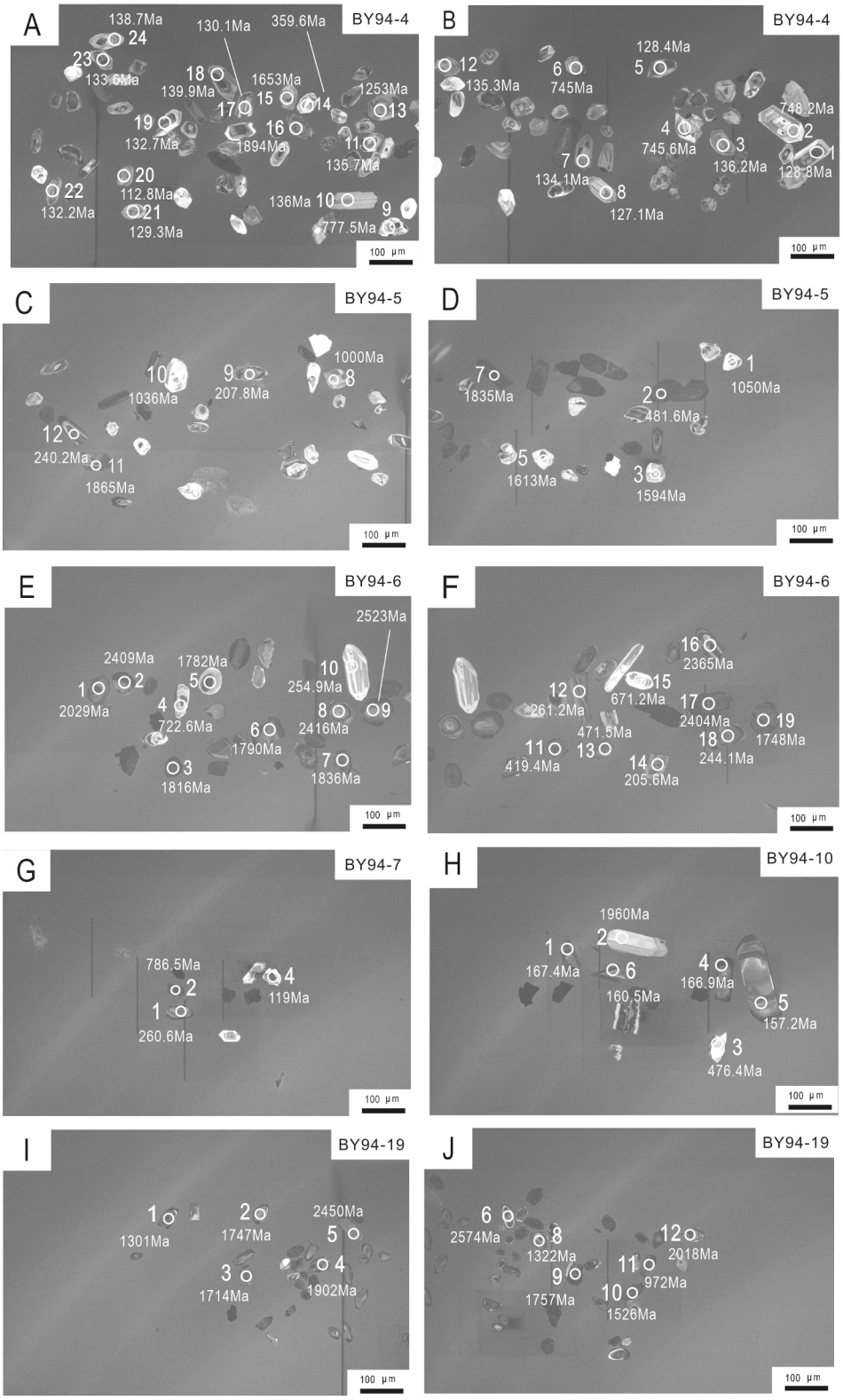


Fig. 12. Cathodoluminescence images of detrital zircons from samples of units H2–H9. (A, B) Sample BY94-4, H9; (C, D) sample BY94-5, H4; (E, F) sample BY94-6, H8; (G, H) samples BY 94-7 and BY 94-10, H8; (I, J) sample BY 94-19, H3.

roughly described as follows. It comprises, in ascending order: unit H1, a dark-gray metamorphosed gravel-bearing coarse-grained feldspar-quartz sandstone interbedded with metamorphosed conglomerate of variable thickness, intercalated with metamorphosed coarse-grained feldspar–quartz sandstone, with parallel bedding and imbricate dark-gray metamorphosed fine-grained feldspar; H2, quartz sandstone including dark-gray or grayish white metamorphosed fine-grained feldspar-quartz sandstone, and grayish white metamorphosed quartz sandstone; H3, argillaceous slate and quartz sandstone; H4, siliceous slate and quartz sandstone; H5, carbonatized argillaceous slate, slate

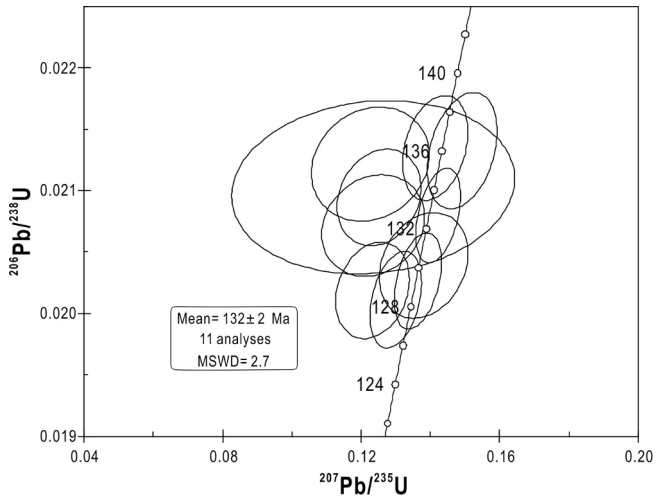


Fig. 13. Zircon SHRIMP U–Pb dating concordia diagram for sample BY94-4 (H9).

intercalated with sandstone, and limestone; H6, carbonatized metamorphosed fine quartz sandstone and metamorphosed medium- to fine-grained quartz sandstone; H7, sandstone interbedded with carbonatite, slate, and microcrystalline limestone; H8, altered coarse- or fine-grained carbonatite; H9, silty slate, carbonaceous siliceous slate, calcareous K-rich slate, with biotitization.

Late Proterozoic units in the West orebody are the same as those in the Main and East orebodies. These units are in conformable contact, apart from unit H8, which intrudes units H3, H4, and H5, with fenitization at the contacts (Liu et al., 2011). Unit H8 was assumed to be the eighth unit in the Bayan Obo Group succession, but units H4 and H8 are in direct contact with a possible thickness of 1000 m (Figs. 4 and 5). Units H5–H7 of the H1–H9 cross-section are missing, and no faults have yet been found to explain their absence between units H8 and H4. This may be due to alteration of the original sedimentary sequence by hydrothermal fluids, resulting in the lack of strata and unconformable contact between units H4 and H8 (Figs. 1, 4, and 5), with high-level syngenetic faults providing upward channels for hydrothermal activity.

Furthermore, the petrology and mineralogy of unit H9 on either side of the syncline hinge are not comparable. Previous work indicates that unit H9 comprises interlayered metadiabase, trachyte, rhyolite dacite, quartzite, dolomite, biotitite, andalusite–biotite hornfels, and carbonaceous sericite slate (Yuan et al., 1995), the first four of which are igneous rocks containing quartzite and dolomite as lenses or interlayers, whereas the latter five have undergone metasomatism or metamorphism. These rocks occur mainly within trachyte or on its margins. Based on a cross-section of the southern margin of the main orebody (Fig. 4) and petrography, this study has shown that the unit comprises mainly trachyte, metadiabase, quartzite, dolomite, biotitite, riebeckite–feldspatite, carbonaceous slate, and altered equivalents. The compact, platy, grey trachyte with a microcrystalline texture has the appearance of siliceous rock with no obvious mineral grains, and had not been studied previously due to limitations on exploration. It is clear now that unit H9 occurs as stratified or stratoid beds dipping southeast and overlying unit H8. It has been partly metamorphosed during the intrusion of unit H8, with the formation of ultramafic dikes, dolomite, and quartz veins. Nb, REE, and Fe mineralization are highly developed in the contact between units H8 and H9, together with the occurrence of biotite, riebeckite–feldspatite, and carbonaceous slate (Fig. 3C, D). Unit H9 thus comprises a series of interlayered igneous rocks, formed before the intrusion of unit H8 (Fig. 3C, D).

It was previously considered that ore mineralization in Bayan Obo is structurally controlled by the Bayan syncline (e.g., Lai et al., 2015 and Yang et al., 2016). It is assumed that the H8 orebody occurs in both limbs of the syncline. The south limb is small and hosts the Dongjiegele orebody, and the much larger north limb hosts the East orebody. However, the above assumption is possibly based on the hypothesis that unit H8 is sedimentary dolomite and correlation of the north and south orebodies is poorly constrained. Based on our field and petrographic studies of the H1–H9 cross-section, the stratigraphic sequence to the north of the syncline is distinct from that in the south (Figs. 4 and 5). Furthermore, deep-drilling exploration indicates that the East orebody is very thick and continuously extend to the deep beyond exploration limitation (Fig. 15). Its steep dipangle (70°–80°) is consistent from surface to depth, with no reduction in dip angle. In contrast, the Dongjiegele orebody is relatively narrow and disseminated. There are major differences between the so-called two limbs in terms of thickness, occurrence, types of ores and their grades and spatial distribution, and they cannot be connected according to the characteristics of synclinal structure. Indeed, the deep-drilling exploration (WK22-02 and WK22-61; Fig. 15) revealed no syncline core at depth. It is therefore likely that the syncline does not exist, with the H8 orebody most likely being a carbonatitic igneous conduit extending to depth.

Earlier field observations by Liu et al. (2012) indicate that the H8 orebody is not layered rock, with no bedding or fixed sequence and, importantly, it intrudes surrounding rock. Le Bas et al. (1997) suggested that the laminar structures of the orebody were due to tectonic deformation, with fenite alteration in unit H8 indicating a magmatic carbonatite origin. The reported stratoid structure is likely a result of magma

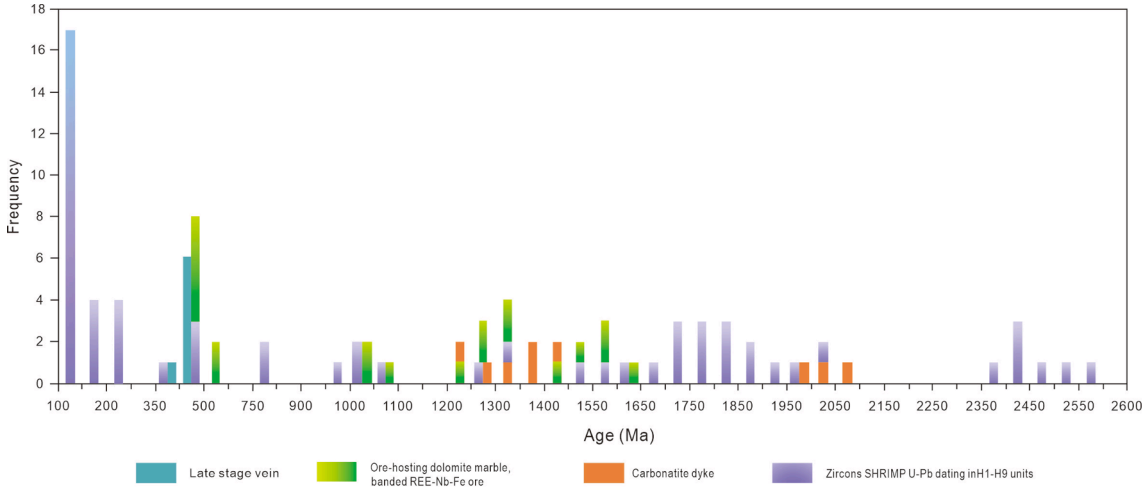


Fig. 14. Frequency distribution of SHRIMP U–Pb ages of samples from units H2–H9 around the Bayan Obo deposit.

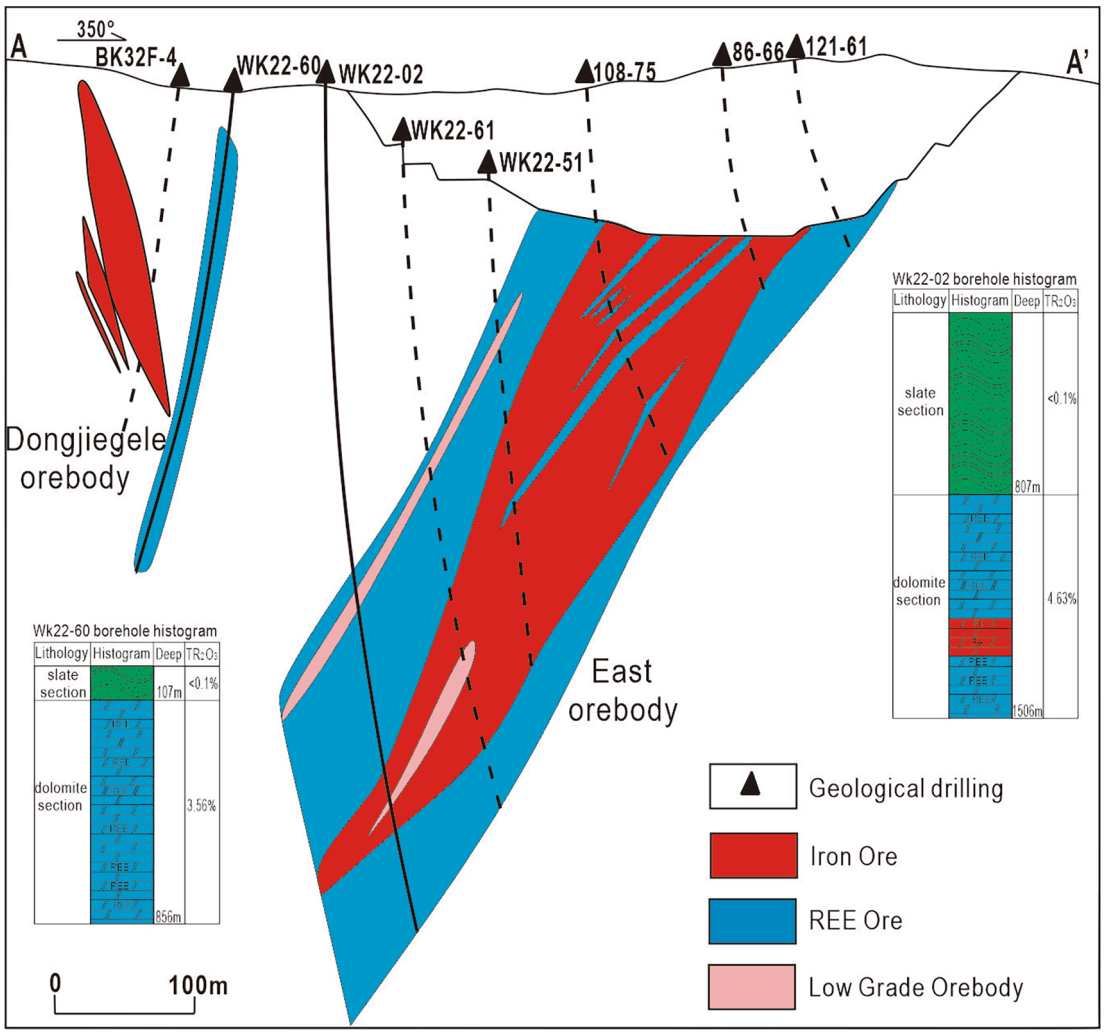


Fig. 15. Cross-section A–A' in Fig. 4, based on deep drilling.

flow rather than sedimentary bedding. Our mineralogy results and previous work (e.g., Yang et al., 2003; Le Bas et al., 2007) indicate that the H8 orebody has mineralogical and whole-rock geochemical characteristics (e.g., high REE, Ba, Th, and Nb) distinct from those of contacting units. Further Sr–Nd–Mg–B geochemical studies also support an igneous origin for the H8 orebody (e.g., Song et al., 2018; Yang et al., 2019; Chen et al., 2020; Kuebler et al., 2020).

5.2. Zircon SHRIMP U–Pb dating and its implications for REE mineralization

Various isotopic systems have been applied to different minerals to determine the formation ages of units H1–H9, yielding the following age data (Table 2): 1675–1648 Ma for H1 (Institute of Geochemistry, Chinese Academy of Sciences, 1988); a Sm–Nd age of 1232 ± 65 Ma for calcite veins in H2 (Zhang et al., 1994); Rb–Sr and U–Pb ages of 730 and 1676 Ma, respectively, for slate in H3 (Xiao, 1979; Jiang, 1982); detrital zircon U–Pb ages of 2596–2379 and 1946–1761 Ma for quartz sandstone in H4 (Yang et al., 2012); and ^{40}Ar–^{39}Ar ages of 1180–640 Ma for alkaline amphibole veins in H6 (Conrad and McKee, 1992). Unit H9 has been dated by the Sm–Nd, K–Ar, Rb–Sr, U–Pb, Hf isotopic systems, yielding ages of 1096 ± 56, 1208 ± 123, 1096, 246–236, 354–314, 1728 ± 5, and 1505 Ma for slate and zircons (Institute of Geochemistry, Chinese Academy of Sciences, 1988; Jiang, 1982; Lai et al., 2015; Liu et al., 2001; Wang et al., 1991; Yuan et al., 2000; Zhang et al., 1997). Here, the ages of detrital zircons from units H2–H8, as determined by SHRIMP analyses, vary considerably between samples from individual units (2574 ± 25 to 132 ± 2 Ma; Supplementary Table 2), overlapping previously reported ages for the Bayan Obo ore field.

As the main host of REE mineralization, unit H8 has been extensively dated using a wide range of methods including whole-rock and mineral Sm–Nd isochron, amphibole Ar–Ar, pyrite Re–Os, and La–Ba isotopic dating, and *in situ* U–Th–Pb zircon and REE analyses (e.g., monazite and bastnäsite), yielding ages of 1683, 1588, 1500, 1400, 1300, 555–398, and 260 Ma (e.g., Institute of Geochemistry, Chinese Academy of Sciences, 1988; Liu et al., 2001, 2004; Song et al., 2018; Wang et al., 1994; Yang et al., 2019; Yuan et al., 1992a,b; Zhang et al., 2003), with frequency-distribution peaks at *ca.* 1.3 Ga and 400 Ma. However, the REE-rich intrusive carbonatite dykes adjacent to the orebodies have a consistent age of *ca.* 1.3 Ga (Yang et al., 2011a; Fan et al., 2014; Zhang et al., 2017).

There is a current consensus that the REE mineralization was originally a product of carbonatite magmatism at *ca.* 1.3 Ga (e.g., Smith et al., 2016; Lai et al., 2015; Song et al., 2018; Yang et al., 2019), most likely related to the breakup of the Columbia supercontinent (Fan et al., 2016) and a late hydrothermal REE re-distribution event. The younger ages (*ca.* 440 Ma) may be related to subduction of the Paleo-Asian oceanic plate during the Silurian (Wang et al., 1994; Chao et al., 1997), but whether the late hydrothermal activity included protracted multiple events or a single episode is still debated. Song et al. (2018) reported single Sm–Nd monazite ages of 913–360 Ma with single-stage evolution, and suggested that the *ca.* 1.3 Ga primary REE ores underwent multiple

Table 2
A summary of previously-reported ages for H2-H9 units in the Bayan Obo deposit.

Unit	Method	Subject	Age (Ma)	References.
H2	Sm-Nd	Carbonate vein	1223 ± 65	Zhang et al. (1994)
H3	Rb-Sr	Dark slate	730	Xiao (1979)
	U-Pb	Dark slate	1676	Jiang (1982)
	U-Pb	Zircons in H3	2574 ± 25 ~ 972 ± 29	this study
H4	U-Pb	Detrital zircon from quartz sandstone	2379 ~ 2596 1761 ~ 1946	Yang et al. (2012)
	U-Pb	Zircons in H4	1865 ± 20 ~ 207.8 ± 2.3	this study
H6	^{40}Ar-^{39}Ar	Cut H6 alkaline amphibole vein	640 ~ 1180	Conrad and McKee (1992)
H8	Th-Pb	Monazite	1683	Institute of Geochemistry, Chinese Academy of Sciences (1988)
	U-Pb	Apatite	1588	Institute of Geochemistry, Chinese Academy of Sciences (1988)
	Pb-Pb	Whole rock and galena	1500	Institute of Geochemistry, Chinese Academy of Sciences (1988)
	Pb-Pb	Dolomite	1500 ± 400	Liu et al. (2001)
	Th-Pb	Monazite and barium-fluorocarbon strontium	555 ~ 398	Wang et al. (1994)
	U-Pb	Zircons in H8	2523 ± 28 ~ 205.6 ± 2.6	this study
	U-Pb	Zircons in H8	1960 ± 29 ~ 157.2 ± 1.9	this study
	U-Pb	Zircons in H8	786.5 ± 8.4 ~ 119 ± 1.4	this study
H9	Sm-Nd	K-rich slate	1096 ± 56	Zhang et al. (1997)
	Sm-Nd	Carbonaceous slate	1208 ± 123	Zhang et al. (1997)
	Sm-Nd	Slate	1096	Yuan et al. (2000)
	K-Ar	Slate	236 ~ 246	Institute of Geochemistry, Chinese Academy of Sciences (1988)
	Rb-Sr	Dark slate	314 ~ 354	Jiang (1982)
	U-Pb	Zirconite rich in potassium slate	1728 ± 5	Wang et al. (1991)
	Model age of Hf	Slate	1505	Lai et al. (2015)
	U-Pb	Zircons in H9	132 ± 2	this study

late hydrothermal modifications induced by Sr-rich, REE-poor metamorphic fluids derived from nearby sedimentary rocks. A recently study by Li et al. (2021) determined monazite and bastnäsite Th–Pb ages clustering at 450–400 or 280–260 Ma, suggesting two discrete episodes of post-ore hydrothermal activity after the primary REE ore was formed at ca. 1.3 Ga. However, Zhu et al., (2015) reviewed Sm–Nd isotopic age data to constrain the chronology of REE mineralization events at Bayan Obo, concluding that the series of ages between 1400 and 400 Ma resulted from thermal disturbances rather than additional mineralization events. Similarly, Campbell et al. (2014) identified zircons from the East orebody with magmatic cores and skeletal rims in CL images, with Th–Pb ages of *ca.* 1.3 Ga and 450 Ma, respectively, suggesting two stages of magmatic to hydrothermal evolution.

Twenty-seven zircon ages were obtained for the H8 orebody in this study, with wide-ranging values of 1960 ± 29, 786.5 ± 8.4, 160.5 ± 1.9, and 119 ± 1.4 Ma (Supplementary Table 2), but most are not consistent with the hydrothermal episodes (400–500 and 260–280 Ma) recorded in the deposit. Recently, Li et al. (2021), using NanoSIMS, found that monazite and bastnäsite in the orebody have commonly undergone fluid-aided alteration, with Pb having been lost or its distribution changed in the altered REE minerals. The ages of minerals thus likely represent partial or total isotopic resetting, with no meaningful geological implications. It seems that relative to the Sm–Nd isotopic system, the U–Th–Pb system is more susceptible to fluid-induced metasomatic alteration (Li et al., 2021). Considering that the zircons studied here lack high U, Th, and Pb contents, and have undergone Pb loss, with 11 zircon ages younger than 200 Ma being acquired from the SHRIMP U–Pb concordia diagram, we suggest that most zircon ages represent fluid-assisted resetting ages, and caution should be exercised in explaining U–Th–Pb dating results for Bayan Obo REE deposits.

6. Conclusions

Our field investigation of the H1–H9 cross-section of the Bayan Obo deposit indicates that units H5–H7 are missing from previously proposed Bayan syncline strata. The occurrences of unit H9 on either side of the syncline are not comparable. Deep-drilling exploration reveals that the East orebody has a steep dip angle and extends continuously to depth with no change in dip, indicating that the syncline does not exist. The mineralogical and REE geochemical characteristics of the H8 orebody are distinct from those of the other units. Based on the reported intrusion of unit H8 in surrounding rock and isotopic geochemistry, we suggest that the H8 orebody is a carbonatitic igneous conduit rather than being of sedimentary origin. U–Pb dating of detrital zircons from units H2–H9 yielded protracted ages from 2574 ± 25 to 132 ± 2 Ma, overlapping those of units H1–H9 and the main REE mineralization periods. These complicated orebody ages represent fluid-assisted resetting ages.

Declaration of Competing Interest

The authors declare that they have no known competing financial interests or personal relationships that could have appeared to influence the work reported in this paper.

Acknowledgments

Three anonymous reviewers are greatly appreciated for their constructive reviews. This research was funded by the Key Special Project for Introduced Talents Team of Southern Marine Science and Engineering, Guangzhou Laboratory (Guangzhou) (Grant GML2019ZD0106), Strategic Priority Research Program of the Chinese Academy of Sciences (Grant XDA20070304), National Natural Science Foundation of China (Grant 41922014, 4172044), Fundamental Research Funds for the Institute of Geology, Chinese Academy of Geological Sciences (Grant J2004) and Geological Survey Program of the China Geological Survey, Ministry of Natural Resources (Grants DD201900660 and DD20211358).

Appendix A. Supplementary data

Supplementary data to this article can be found online at https://doi.org/10.1016/j.oregeorev.2021.104397.

References

Broom-Fendley, S., Styles, M.T., Appleton, J.D., Gunn, G., Wall, F., 2016. Evidence for dissolution-reprecipitation of apatite and preferential LREE mobility in carbonatite-derived late-stage hydrothermal processes. Am. Min. 101, 596–611.Butera, K.M., Williams, I.S., Blevin, P.L., Simpson, C.J., 2004. Zircon U-Pb dating of early palaeozoic monzonitic intrusives from the Goonumbla area, New South Wales. Aust J Earth Sci 48, 457–464.

Campbell, L.S., Compston, W., Sircombe, K.N., Wilkinson, C.C., 2014. Zircon from the East Orebody of the Bayan Obo Fe-Nb-REE deposit, China, and SHRIMP ages for carbonatite-related magmatism and REE mineralization events. Contrib. Miner. Petrol. 168, 1040–1062.

Cao, R.L., Zhu, S.H., Wang, J.W., 1994. Source materials for the Bayan Obo Fe-REE ore deposit and problems of the genetic theory. Sci. China. 24, 1298–1307 (in Chinese with English abstract).

Castor, S.B., 2008. The Mountian Pass rare-earth carbonatite and associated ultrapotassic rocks. California. Can. Mineral. 46, 779–806.

Chakhmouradian, A.R., Wall, F., 2012. Rare earth elements: minerals, mines, magnets (and more). Elements 8, 333–340.

Chao, E.C.T., Back, J.M., Minkin, J.A., Ren, Y., 1992. Host-rock controlled epigenetic, hydrothermal metasomatic origin of the Bayan Obo REE-Fe-Nb ore deposit, Inner Mongolia, P.R.C. Appl. Geochem. 7, 443–458.

Chao, E.C.T., Back, J.M., Minkin, J.A., Tatsumoto, M., Wang, J.W., Conrad, J.E., Mckee, E.H., 1997. The sedimentary carbonatite-hosted giant Bayan Obo REE-Fe-Nb ore deposit of Inner Mongolia, China: cornerstone examples for giant polymetallic ore deposits of hydrothermal origin. USGS Bull. 2143, 65.

Chao, E.C.T., Tatsumoto, M., Minkin, J., Back, J.M., McKee, E.H., Ren, Y.C., Li, G.M., 1991. A variety of evidence to establish the mineral sequences of ore-forming minerals of Bayan Obo rare earth ore deposit. Contrib. Geol. Miner. Resour. Res. 6, 1–7 (in Chinese).

Chen, W., Liu, H.Y., Lu, J., Jiang, S.Y., Simonetti, A., Xu, C., Zhang, W., 2020. The formation history of the ore-bearing dolomite marble from the giant Bayan Obo Fe-REE-Nb deposit, Inner Mongolia: insights from micron-scale geochemical data. Miner. Deposita. 55, 131–146.

Conrad, J.E., McKee, E.H., 1992. $^{40}Ar/^{39}Ar$ dating of vein amphibole from the Bayan Obo iron-rare earth element-niobium deposit, China-Constraints on mineralization and deposition of the Bayan Obo Group. Econ. Geol. 87, 185–188.

Drew, L.J., Meng, Q.R., Sun, W.J., 1990. The Bayan Obo iron-rare-earth-niobium deposits, Inner Mongolia. China. Lithos. 26, 43–65.

Fan, H.R., Hu, F.F., Wang, K.Y., Liu, Y.S., 2009. Geochronology framework of late Paleozoic dioritic-granitic plutons in the Bayan Obo area, Inner Mongolia, and tectonic significance. Acta Petrologica Sinica. 25, 2933–2938.

Fan, H.R., Hu, F.F., Yang, K.F., Pirajno, F., Liu, X., Wang, K.Y., 2014. Integrated U-Pb and Sm–Nd geochronology for a REE-rich carbonatite dyke at the giant Bayan Obo REE deposit. Northern China. Ore Geol. Rev. 63, 510–519.

Fan, H.R., Yang, K.F., Hu, F.F., Liu, S., Wang, K.Y., 2016. The giant Bayan Obo REE-Nb-Fe deposit, China: Controversy and ore genesis. Geosci. Front. 7, 335–344.

Gunn, A.G. (Ed.), 2014. Critical Metals Handbook. Wiley, New York.

Hou, Z.Q., Cook, N.J., 2009. Metallogenesis of the Tibetan collisional orogen: A review and introduction to the special issue. Ore Geol. Rev. 36, 2–24.

Hu, F.F., Fan, H.R., Liu, S., Yang, K.F., Chen, F., 2009. Samarium-neodymium and rubidium- strontium isotopic dating of veined REE mineralization for the Bayan Obo REE-Nb-Fe deposit, Northern China. Resour. Geol. 59, 407–414.

Jia, Y.H., Liu, Y., 2019. REE Enrichment during Magmatic-Hydrothermal Processes in Carbonatite-Related REE Deposits: A Case Study of the Weishan REE Deposit. China. Minerals 10, 25.

Jia, Y.H., Liu, Y., 2020. Factors controlling the generation and diversity of giant carbonatite-related rare earth element deposits: insights from the Mianning-Dechang belt. Ore Geol. Rev. 12, 103472.

Jiang, C.W., 1982. Isotope geology of the Bayan Obo deposit. Geol. Sci. 1982, 270–276 (in Chinese).

Kuebler, C., Simonetti, A., Chen, W., Simonetti, S.S., 2020. Boron isotopic investigation of the Bayan Obo carbonatite complex: Insights into the source of mantle carbon and hydrothermal alteration. Chem. Geol. 557, 119859.

Lai, X.D., Yang, X.D., Liu, Y.L., Yan, Z.Q., 2016. Genesis of the Bayan Obo Fe-REE-Nb deposit: Evidences from Pb-Pb age and microanalysis of the H8 Formation in Inner Mongolia, North China Craton. J. Asian Earth Sci. 120, 87–99.

Lai, X.D., Yang, X.Y., Santosh, M., Liu, Y.L., Ling, M.X., 2015. New data of the Bayan Obo Fe-REE-Nb deposit, Inner Mongolia: Implications for ore genesis. Precambr. Res. 263, 109–122.

Lai, X.D., Yang, X.Y., Sun, W.D., 2013. Geochemical constraints on genesis of dolomite marble in the Bayan Obo REE–Nb–Fe deposit, Inner Mongolia: Implications for REE mineralization. J. Asian Earth Sci. 57, 90–102.

Le Bas, M.J., Spiro, B., Yang, X., 1997. Oxygen, carbon and strontium isotope study of the carbonatitic dolomite host of the Bayan Obo Fe-Nb-REE deposit, Inner Mongolia. N. China. Mineral. Mag. 61, 531–541.

Le Bas, M.J., Yang, X.M., Taylor, R.N., Spiro, B., Milton, J.A., Peishan, Z., 2007. New evidence from a calcite-dolomite carbonatite dyke for the magmatic origin of the massive Bayan Obo ore-bearing dolomite marble, Inner Mongolia. China. Mineral. Petrol. 90, 223–248.

Li, G.W., Li, Q.F., Jiang, W.D., 1996. Multiple classification and correlation of the stratigraphy of China (15): Stratigraphy (Lithostratic) of Nei Mongol Autonomous Region. China University of Geosciences Press, Wuhan (in Chinese).

Li, M., 1959. The Geology and Exploration of Bayan Obo Iron Ore Deposit. Geological Publishing House, Beijing.

Li, X.C., Yang, K.F., Spandler, C., Fan, H.R., Zhou, M.F., Hao, J.L., Yang, Y.H., 2021. The effect of fluid-aided modification on the Sm-Nd and Th-Pb geochronology of monazite and bastnäsite: Implication for resolving complex isotopic age data in REE ore system. Geochimica et Cosmochimica Acta. 300, 1–24.

Institute of Geochemistry, Chinese Academy of Sciences. 1988. Geochemistry of the Bayan Obo Ore Deposit. Science Press, Beijing, pp. 72 (in Chinese).

Ling, M., X., Zhang, H., Li, H., Liu, Y.L., Liu, J., Li, L.Q., Li, C.Y., Yang, X.Y., Sun, W., 2014. The Permian-Triassic granitoids in Bayan Obo, North China Craton: A geochemical and geochronological study. Lithos 190: 430-439.

Liu, C.H., Zhao, G.C., Liu, F.L., Shi, J.R., 2017. Detrital zircon U-Pb and Hf isotopic and whole-rock geochemical study of the Bayan Obo Group, northern margin of the North China Craton: implications for Rodinia reconstruction. Precambr. Res. 303, 372–391.

Liu, J., Li, Y., Ling, M., Sun, W., 2011. Chronology and geological significance of the basement rock of the giant Bayan Obo REE-Nb-Fe ore deposit. Geochimica 40, 209–222.

Liu, J.Y., Su, S.W., Zhang, T.R., Zhang, Y.X., 2006. A Discussion on the Practicability of Prospecting in the Deep Part of the East Mine and Kernel Part of the Bayan Syncline, Bayan Obo Ore Field. Geological Review, 52(6): 821–825 (In Chinese, English abstract).

Liu, T.G., Zhang, Z.W., Ye, L., Shan, N.P., Yang, Z.F., Li, C.X., Feng, J.R., 2012. Geological and geochemical charactertics and genesis of “dolomite” at Bayan Obo, China. Acta Geologica Sinica 5, 47–58.

Liu, Y., Hou, Z.Q., 2017. A synthesis of mineralization styles with an integrated genetic model of carbonatite-syenite-hosted REE deposits in the Cenozoic Mianning-Dechang REE metallogenic belt, the eastern Tibetan Plateau, southwestern China. J. Asian Earth Sci. 137, 35–79.

Liu, Y., Yang, G., Chen, J., Du, A., Xie, Z., 2004. Re-Os dating of pyrite from Giant Bayan Obo REE-Nb-Fe deposit. Chin. Sci. Bull. 49, 2627–2631.

Liu, Y.F., Bagas, L., Nie, F.J., Jiang, S.H., Li, C., 2016. Re-Os system of black schist from the Mesoproterozoic Bayan Obo Group, Central Inner Mongolia, China and its geological implications. Lithos 261, 296–306.

Liu, Y., Chakhmouradian, A.R., Hou, Z.Q., Song, W.L., Kynický, J., 2019a. Development of REE mineralization in the giant Maoniuping deposit (Sichuan, China): insights from mineralogy, fluid inclusions, and trace-element geochemistry. Miner. Deposita. 54, 701–718.

Liu, Y., Hou, Z.Q., Zhang, R.Q., Wang, P., Gao, J.F., Raschke, M.B., 2019b. Zircon alteration as a proxy for rare earth element mineralization processes in carbonatite-nordmarkite complexes of the mianning-dechang rare Earth element belt, China. Econ. Geol. 114 (4), 719–744.

Liu, Y.L., Chen, J.F., Li, H.M., Qian, H., Xiao, G.W., Zhang, T.R., 2005. Single-grain U-Th-Pb-Sm-Nd dating of monazite from dolomite type ores of the Bayan Obo deposit. Acta Petrol. Sin. 21, 881–888 (in Chinese with English abstract).

Liu, Y.L., Peng, G.Y., Zhang, Y., Li, H.M., Chen, J.F., 2001. U-Pb and Pb-Pb dating of ore-hosting H8 dolomite at Bayan Obo. Bull. Mineral. Petrol. and Geochem. 20, 274–277 (in Chinese with English abstract).

Meng, Q., 1982. The genesis of the host rock dolomite of Bayan Obo iron deposits and the analysis of its sedimentary environment. Geol. Rev. 28, 481–489 (In Chinese with English Abstract).

Ren, Y., Yang, X., Wang, S., Ozturk, H., 2019. Mineralogical and geochemical study of apatite and dolomite from the Bayan Obo giant Fe-REE-Nb deposit in Inner Mongolia: new evidences for genesis. Ore Geo. Rev. 109, 381–406.

Ren, Y., Zhang, Y., Zhang, Z., 1994. Study on heat events of ore forming in the Bayan Obo deposit. Sci. Geol. Sin. 29, 95–101 (in Chinese with English abstract).

Smith, M.P., Moore, K., Kavecsanszki, D., Finch, A.A., Kynicky, J., Wall, F., 2016. From mantle to critical zone: A review of large and giant sized deposits of the rare earth elements. Geosci. Front. 7, 315–334.

Song, W.L., Xu, C., Smith, M.P., Chakmouradian, A.R., Brenna, M., Kynicky, J., Chen, W., Yang, Y.H., Deng, M., Tang, H.Y., 2018. Genesis of the world’s largest rare earth element deposit, Bayan Obo, China: protracted mineralization evolution over ~1 b. y. Geology 46, 323–326.

Sun, J., Fang, N., Li, S.Z., Chen, Y.L., Zhu, X.K., 2012. Magnesium isotopic constraints on the genesis of Bayan Obo ore deposit. Acta. Petrologica. Sinca. 28 (9), 2890–2902.

Wall, F., 2014. Rare Earth Elements. In: Gunn, A. (Ed.), Critical Metals Handbook. Wiley, New York.

Wang, J., Sun, Y.F., Lu, S.N., Li, H.M., 1991. Results of U-Pb dating of single zircon from the Bayan Obo Group and its geological significance. In: compilation of abstract papers for the academic conference on Isotopic geochronology of the Precambrian in Northern China. 25-27 (in Chinese).

Wang, J.W., Tasumoto, M., Li, X.B., Premo, W.R., Chao, E.T.C., 1994. A precise $^{232}Th/^{208}Pb$ chronology of fine-grained monazite, age of the Bayan Obo REE-Fe-Nb ore deposit. China. Geochim. Cosmochim. Acta. 58, 3155–3169.

Wang, K., Fang, A., Zhang, J., Yu, L., Dong, C., Zan, J., Yu, L., Dong, C., Zan, J., Hao, M., & Hu, F. (2019). Genetic relationship between fenitized ores and hosting dolomite carbonatite of the Bayan Obo REE deposit, Inner Mongolia, China. J. Asian Earth Sci. 174, 189-204.

Weng, Z.H., Jowitt, S.M., Mudd, G.M., Haque, N., 2015. A detailed assessment of global rare earth element resources: opportunities and challenges. Econ. Geol. 110, 1925–1952.White, L.T., Ireland, T.R., 2003. High-uranium matrix effect in zircon and its implications for SHRIMP U-Pb age determinations. Chem. Geol. 88, 1336–1344.

White, L.T., Ireland, T.R., 2012. High-uranium matrix effect in zircon and its implications for shrimp U-Pb age determinations. Chemical Geology 306–307, 78–91.

Xiao, Z.Y., 1979. Discussion on isotope age data in Bayan Obo mining area. Proceedings of national Isotope geology Conference, Geology publication 2–28 (in Chinese).

Xie, Y.L., Qu, Y.W., Yang, Z.F., Liang, P., Zong, R.C., Wang, Q.W., Xia, J.M., Li, B.C., 2019. Giant Bayan Obo Fe-Nb-REE deposit: Progresses, Controversaries and new understandings. Miner. Deposits. 38, 983–1003 (in Chinese).
Xu, C., Kynicky, J., Chakhmouradian, A.R., Li, X., Song, W., 2015. A case example of the importance of multi-analytical approach in deciphering carbonatite petrogenesis in South Qinling orogen: Miaoya rare-metal deposit, centra China. Lithos. 227 (107), 121.
Xu, C., Taylor, R.N., Li, W., Kynicky, J., Chakhmouradian, A.R., Song, W.L., 2012. Comparison of fluorite geochemistry from REE deposits in the Panxi region and Bayan Obo. China. J. Asian Earth Sci. 57, 76–89.
Yang, K.F., Fan, H.R., Hu, F.F., Wang, K.K., 2012. Sediment Source of Bayan Obo Marginal Rift and Genesis of Ore-Bearing Dolomite of the Giant REE Deposit. Acta Geosci. Sin. 86, 775–784 (in Chinese).
Yang, K.F., Fan, H.R., Pirajno, F., Li, X.C., 2019. The Bayan Obo (China) giant REE accumulation conundrum elucidated by intense magmatic differentiation of carbonatite. Geology. 47, 1198–2102.
Yang, K.F., Fan, H.R., Santosh, M., Hu, F.F., Wang, K.Y., 2011a. Mesoproterozoic carbonatitic magmatism in the Bayan Obo deposit, Inner Mongolia, North China: constraints for the mechanism of super accumulation of Rare Earth Elements. Ore Geol. Rev. 40, 122–131.
Yang, K.F., Fan, H.R., Santosh, M., Hu, F.F., Wang, K.Y., 2011b. Mesoproterozoic carbonatitic magmatism in the Bayan Obo deposit, Inner Mongolia, North China: Constraints for the mechanism of super accumulation of rare earth elements. Ore Geol. Rev. 40, 122–131.
Yang, X.M., Le Bas, M.J., 2004. Chemical compositions of carbonate minerals from Bayan Obo, Inner Mongolia, China: implications for petrogenesis. Lithos. 72, 97–116.
Yang, X.M., Yang, X.Y., Zheng, Y.F., Le Bas, M.J., 2003. A rare earth element-rich carbonatite dyke at Bayan Obo, Inner Mongolia, North China. Mineral. Petrol. 78, 93–110.
Yang, X.Y., Lai, X.D., Pirajno, F., Liu, Y.L., Ling, M.X., Sun, W.D., 2016. Genesis of the Bayan Obo Fe-REE-Nb formation in Inner Mongolia, North China Craton: A perspective review. Precambr. Res. 288, 39–71.
Yang, X.Y., Sun, W.D., Zhang, Y.X., Zheng, Y.F., 2009. Geochemical constraints on the genesis of the Bayan Obo Fe–Nb–REE deposit in Inner Mongolia. China. Geochim. Cosmochim. Acta. 73, 1417–1435.
Ye, H.M., Li, X.H., Lan, Z.W., 2013. Geochemical and Sr–Nd–Hf–O–C isotopic constraints on the origin of the Neoproterozoic Qieganbulake ultramafic–carbonatite complex from the Tarim Block, Northwest China. Lithos 182–183, 150–164.
Yuan, Z., Bai, G., Wu, C., Zhang, Z., Ye, X., 1992a. Geological features and genesis of the Bayan Obo REE ore deposit, Inner Mongolia, China. Applied Geochemistry 7, 429–442.
Yuan, Z.X., Bai, G., Wu, C., 1995. The petrological features of volcanic rocks in H9 formation of the Bayan Obo ore district, Inner Mongolia and geological significance. Miner Deposits. 14, 197–205 (in Chinese).
Yuan, Z.X., Bai, G., Wu, C.Y., Zhang, Z.Q., Ye, X.J., 1992b. Geological features and genesis of the Bayan Obo deposit, Inner Mongolia. China. Appl. Geochem. 7, 429–442.
Yuan, Z.X., Bai, G., Zhang, Z.Q., 2000. Trachytic rock and associated fenitization in the Bayan Obo ore deposit, Inner Mongolia, China: evidence formagmatic–hydrothermal mineralization related to a carbonatitic complex. Acta Geol. Sin. Engl. Ed. 74, 148–153.
Zhang, S.H., Zhao, Y., Liu, Y., 2017. A precise zircon Th-Pb age of carbonatite sills from the world's largest Bayan Obo deposit: Implications for timing and genesis of REE-Nb mineralization. Precambrian Res. 291, 202–219.
Zhang, Z.Q., Tang, S.H., Chen, Q.T., Wang, J.H., 1997. Sm-Nd ages and origins of metamorphic rocks for the H9 formation in the Bayan Obo ore district, and relationship with the ore forming event. Acta Geosci. Sin. 18, 267–274 (in Chinese).
Zhang, Z.Q., Tang, S.H., Wang, J.H., Yuan, Z.X., Bai, G., 1994. New data for ore-forming age of the Bayan Obo REE deposit. Inner Mongolia. Acta Geosci. Sin. 29, 85–94 (in Chinese).
Zhang, Z.Q., Tang, S.H., Wang, J.H., Yuan, Z.X., Bai, G., 2003. Information about ore deposit formation in different epochs: Age of the west orebodies of the Bayan Obo deposit with a discussion. Geology in China 30, 130–137 (in Chinese).
Zhang, Z.Q., Tang, S.H., Yuan, Z.X., Bai, G., Wang, J.H., 2001. The Sm-Nd and Rr-Sr isotopic systems of the dolomites in the Bayan Obo deposit in Inner Mongolia. Acta Petrol. Sin. 17, 637–642.
Zhao, C., 2014. Comparison between the East Jie Le Gele orebody and the East orebody in the measured geological section of Bayan Obo Ore Field and preliminary study on syncline structure. Mineral Deposits S1, 161–162 (in Chinese).
Zhong, Y., Zhai, M.G., Peng, P., Santosh, M., Ma, X., 2015. Detrital zircon U-Pb dating and whole-rock geochemistry from the clastic rocks in the northern marginal basin of the North China Craton: constraints on depositional age and provenance of the Bayan Obo Group. Precambr. Res. 258, 133–145.
Zhu, X.K., Sun, J., Pan, C.X., 2015. Sm-Nd isotopic constraints on rare-earth mineralization in the Bayan Obo ore deposit, Inner Mongolia. China. Ore Geol. Rev. 64, 543–553.